NONLINEAR ROTORDYNAMICS

ANALYSIS

CONTRACT NAS8-36475

for the period
1 June 1985 - 15 June 1986

Performed for
NASA Marshall Space Flight Center

Performed by

Department of Computer Science and Engineering
Auburn University
Auburn University, AL 36849

Principal Investigator: William B. Day

Authors: William B. Day
Richard A. Zalik

ABSTRACT

This Report examines three analytic consequences of the nonlinear Jeffcott equations. The primary application of these analyses is directed toward understanding the excessive vibrations recorded in the LOX pump of the SSME during hot firing ground testing.

The first task is to provide bounds on the coefficients of the equations which delimit the two cases of the numerical solution as a circle or an annulus.

The second task examines the mathematical generalization to multiple forcing functions, which includes the special problems of mass imbalance, side force, rubbing, and combinations of these forces.

Finally, stability and boundedness of the steady-state solutions is discussed and related to the corresponding linear problem.

List of Figures

List of Tables

1. INTRODUCTION

Beginning with Jeffcott's description of a rotating shaft's natural frequency of lateral vibration [6], investigators have sought mathematical explanations of observed vibrations in rotating machinery. In the linear model of the motion of the shaft's center of mass, only the frequency at which the shaft is being driven appears in the steady-state solution except in one special case where the natural frequency is exactly equal to the square root of the ratio of the cross-stiffness and the damping. Otherwise, the solution from the homogenous equation, the transcient portion of the solution, either grows without bound, the case of an unbounded solution, or it decays to zero, the case of a bounded solution.

One of the earliest investigators of rotordynamics which included deadband was Yomamoto [8]. In the rotor, deadband refers to the load carriers (ball bearings) and physically describes the clearance between the outer race of the bearing and the support housing. Yomamoto's work assumes that the response is simply a perturbation of the forcing function. This is tantamount to assuming that one always has the solution graphically depicted as a circle. Straight-forward numerical solutions using a Runge-Kutta Fourth Order technique refute this assumption. Both empirical results by Childs [1, 2] and Gupta et al. [5] as well as numerical solutions by Control Dynamics Company [3] have provided insight in understanding the nonlinear rotor's motion.

It was shown earlier [4] for the nonlinear Jeffcott equation, in which the nonlinearity in induced by deadband and appears in the equations in the form $(1 - \delta/r)w$, that the equation possesses an analytic flexibility which provides a capability of producing a contribution to the steady-state solution whenever the ratio of the cross-stiffness to the damping lies between the values of the square root of the seal stiffness and the square root of the sum of the seal stiffness and the bearing stiffness (the natural frequency).

This Report extends the earlier work in several directions. First, it is necessary to generalize mathematically the Jeffcott equations to allow multiple forcing functions and to examine the implications of these extensions to the asymptotic expansions one uses in approximating the

solution of the equations. Section 2 contains a summary of earlier analytic derivations and the necessary extensions for asymptotic expansions. It is also shown in Section 2 that the cases of mass imbalance, side force, rubbing and any combination of these forcing functions are all special cases of the multiple forcing function problem.

It was shown in [4] that the nonlinear frequency, that frequency which arises when the homogeneous equation provides a part of the total steady-state solution, can be absent or present depending on the magnitude of the forcing function. Section 3 of this Report contains two theorems which provide inequalities on the coefficients of the differential equations and the magnitude of the forcing function. These inequalities are useful in deciding a priori whether a given set of equation parameters will produce a steady-state response which depends solely on the forcing function (graphically, a circle) or a response which also includes a nonlinear frequency term (graphically, an annulus). Several numerical examples along with frequency-response curves are then studied in light of these theorems.

Section 4 begins the numerical investigation of the multiple forcing functions problem vis-a-vis the asymptotic results. In this Section the driving forces are side force and mass imbalance, the most intensely studied special case. Explanations for results from the Final Report of Control Dynamics Company [3] are provided. Section 5 then considers more general numerical examples.

Section 6 deals with boundedness and stability. Two theorems along with a novel mathematical representation of the Jeffcott equations are presented. New boundedness results are also studied by comparing the nonlinear solution's behavior with that of the corresponding linear problem ($\delta = 0$). Finally numerical results are included to illustrate the conjecture that the nonlinear solution's boundedness is predicted by that of the linear solution.

Section 7 contains the conclusion of this Report and opens a can of worms by observing that heretofore the initial conditions have been ignored as a vital factor in determining the analytic solution.

2. SUMMARY OF THE SINGLE FORCING FUNCTION PROBLEM AND EXTENSION TO MULTIPLE FORCING FUNCTIONS

This section contains four subsections which include a summary of the analytic approximations of the Jeffcott equations with a single forcing function, as presented in [4], and new extensions to the Jeffcott equations with multiple forcing functions. Subsection 2.1 presents the dimensional Jeffcott equations and the transformations leading to the nondimensional form and the complex form of these equations. Subsection 2.2 is concerned with the generalization of the complex Jeffcott equation and with the identification of the special cases of mass imbalance, side force, rubbing and combinations of these three forces. Subsection 2.3 is a reproduction from [4] of the arguments leading to the discovery of the nonlinear natural frequency. Subsection 2.4 discusses the application of the method of multiple scales to approximate analytically the solution of the Jeffcott equations when they are forced by a single or by multiple forcing functions. This subsection concludes with a typical example which illuminates the analytic derivations.

2.1 NONDIMENSIONALIZATION

The nonlinear Jeffcott equations which describe the displacement of the rotor center from its equilibrium position in the inertial, Cartesian coordinate system (y, z) (each in meters) and which include bearing forces which hold the rotor in position, are these:

$$\ddot{y} + (C_s/m)\dot{y} + (1/m)\,[K_s + K_B\,(1 - \delta/r)]\,y + (Q_s/m)z = u\omega^2\cos\omega t \qquad (1)$$

$$\ddot{z} + (C_s/m)\dot{z} - (Q_s/m)y + (1/m)\,[K_s + K_B\,(1 - \delta/r)]z = u\omega^2\sin\omega t \qquad (2)$$

when $r = \sqrt{y^2 + z^2} \geq \delta$; otherwise, $K_B = 0$. Here the shaft of the rotor lies along the x-axis and

m = mass (kg.)

C_s = seal damping (kg./s.)

K_s = seal stiffness (kg./s.^{2})

Q_s = cross-coupling stiffness of seal (kg./s.^{2})

u = displacement of the shaft center of mass from the geometric center (m.)

K_B = bearing stiffness (kg./s.^{2})

δ = clearance or deadband between housing and bearing (m.)

μ = coefficient of friction between housing and bearing (none).

ω = angular velocity of the shaft (rad./s.)

Since μ is nondimensional and typically small, one may regard it as zero without affecting the qualitative results. Equations (1) and (2) can be put in nondimensional form using a displacement g and a frequency σ. One pair of candidates for g and σ would be $g = \delta$, the deadband size, and $\sigma^2 = \omega_0^2 = K_s + K_B$, the natural frequency of the corresponding linear problem ($\delta = 0$). Thus, using $Y = y/g$, $Z = z/g$, and $\tau = \sigma t$, the dimensionless equations are these:

$$Y'' + CY' + [A + k(1 - \Delta/R)]\, Y + BZ = E\phi^2 \cos\phi\tau \qquad (3)$$

$$Z'' + CZ' - BY + [A + k(1 - \Delta/R)]\, Z = E\phi^2 \sin\phi\tau \qquad (4)$$

where prime denotes differentiation with respect to τ and $C = C_s/m/\sigma$, $A = K_s/m/\sigma^2$, $k = K_B/m/\sigma^2$, $B = Q_s/m/\sigma^2$, $\Delta = \delta/g$, $R = r/g$, $E = u/g$, and $\phi = \omega/\sigma$.

Equations (3) - (4) can be reduced to the following single equation by defining $W = Y + iZ$;

$$W'' + CW' + \{A + k\,(1 - \Delta/|W|) - iB\}W = E\phi^2 \exp(i\phi\tau). \qquad (5)$$

2.2 GENERALIZATIONS

A generalization of equation (5) is

$$W'' + CW' + AW + K(1 - \Delta/|W|)W = \sum_{n=1}^{L} F_n(\phi_n) \exp(i\phi_n\tau) \qquad (6)$$

where C, A, and K are complex constants and where the nonlinear left-hand side of equation (6) is being driven on the right-hand side by multiple forces. The following are special cases of physical interest:

a. Forcing function is mass imbalance. This is the case derived in equation (5) and is obtained from equation (6) with $L = 1$ and $F_1(\phi_1) = E\phi_1^2$.

b. Forcing function is side force. This force may be introduced into the Jeffcott equations (1) - (2) as a constant replacement for the mass imbalance. In such cases, equation (5) becomes

$$W'' + CW' + \{A + k(1 - \Delta/|W|) - iB\}\, W = \text{constant}.$$

Thus, a side force is the special case of equation (6) with $L = 1$, $F_1(\phi_1) =$ constant, and $\phi_1 = 0$.

c. Forcing function is rubbing. Contact between a rotor and its housing produces a Coulomb damping force. This force would modify the original Jeffcott equations by the addition of the terms:

$$K_{st}(1 - \delta/r)y - \mu K_{st}(1 - \delta/r)\, z + K_{st}(1 - \delta/r)G$$

and $\mu K_{st}(1 - \delta/r)y + K_{st}(1 - \delta/r)\, z + \mu K_{st}(1 - \delta/r)G$

respectively, to the right-hand sides of equations (1) - (2). Here, G = constant = stator offset in the y - direction, K_{st} = stator stiffness and μ = coefficient of friction, which may not be small. As before these forces would be included only when $r = (y^2 + z^2)^{\frac{1}{2}} > \delta$. On replacing y - G by y, equation (5) (and correspondingly its equivalent forms) again occurs but with these modifications:

1. i[-B] is replaced by $i[-B + \mu(K_{st}/g^2)(1 - \Delta/R)]$
2. the forcing function $E\phi^2 \exp(i\phi\tau)$ is replaced by $E\phi^2 \exp(i\phi\tau) + (-\omega_0^2/g^2)(G/\delta)$.

Thus, rubbing is equivalent to having two forcing functions in equation (6) where L = 2, $F_1(\phi_1) = E\phi_1^2$, $F(\phi_2)$ = constant, and $\phi_2 = 0$.

d. Any combination of mass imbalance, side force, and rubbing.

Initially, attention is restricted to equation (5); i.e., equation (6) with L = 1. It will be seen later that in a first approximation, the more complicated cases of L > 1 can be solved as a superposition of the individual responses which are found using equation (5).

2.3 NONLINEAR NATURAL FREQUENCY

Consider the dimensional, homogeneous (E = 0) equation corresponding to equation (5):

$$\ddot{w} + (C_s/m)\dot{w} + (1/m)\{[K_s + K_B(1 - \delta/r) - iQ_s]\}\, w = 0, \qquad (7)$$

where w = y + iz. If this equation were also linear ($\delta = 0$), then exponentially growing or decaying solutions would generally result for a given set of system parameters. In the special case that $(Q_s/C_s)^2 = K_s + K_B$, a sinusoidal solution is obtained with frequency $\beta_0 = Q_s/C_s$. To see this, consider the characteristic equation for w = exp (pt):

$$p^2 + C_s p + [K_s + K_B - iQ_s] = 0$$

$$p = -C_s/2 \pm \{C_s^2/4 - K_s - K_B + iQ_s\}^{\frac{1}{2}}$$

$$= -C_s/2 \pm \{C_s^2/4 - (Q_s/C_s) + iQ_s\}^{\frac{1}{2}}$$

$$= -C_s/2 + i\{iC_s/2 - Q_s/C_s\}$$

$$= -C_s - iQ_s/C_s,\ iQ_s/C_s.$$

In the nonlinear, homogeneous problem, K_B is replaced by $K_B(1 - \delta/r)$; hence, if r is a constant, then there is a wide spectrum of r for which $(Q_s/C_s)^2$ may be $K_s + K_B\ (1 - \delta/r)$; i.e., if

$$K_s < (Q_s/C_s)^2 <= K_s + K_B, \qquad (8)$$

then there is a constant value of r (with $r > \delta$) for which $(Q_s/C_s)^2 = K_s + K_B\ (1 - \delta/r)$. This value of r is denoted by a and the corresponding frequency by $\beta_0 = Q_s/C_s$. This frequency is labeled the nonlinear natural frequency. Thus, whenever inequality (8) is satisfied, equations (1) - (2) with u = 0 have steady-state solutions $y = a \cos(\beta_0 t)$ and $z = a \sin(\beta_0 t)$.

Notice that $\beta_0 = Q_s/C_s <= (K_s + K_B)^{\frac{1}{2}} = \omega_0$, the dimensional natural frequency of the linear system. Thus, in considering the general nonhomogeneous problem, it is necessary to be aware of these three dimensional frequencies:

β_0 - the nonlinear natural frequency,

ω_0 - the natural frequency,

ω - the driving frequency.

It will be shown in the next section that the nonlinear frequency β which may appear in a stable solution of the non-homogeneous version of equation (6) always lies between β_0 and ω_0.

One final rearrangement of equation (5) is made here to emphasize the nonlinear natural frequency:

$$W'' + CW' + \kappa W = \varepsilon f(W) + E\phi^2 \exp(i\phi\tau) \qquad (9)$$

where $\kappa = A + k\ (1 - \Delta/a) - iB$ and $f(W) = k\Delta[1/|W| - 1/a]W/\varepsilon$.

2.4 METHOD OF MULTIPLE SCALES

This section deals with formal, singular asymptotic expansions of the Jeffcott equations as written in equation (9). A straight-forward

asymptotic expansion is not general enough for this problem since it always leads to a zero-order approximation of the form:

$$W = M \exp(i\beta_0\tau) + N \exp(i\phi\tau)$$

for constant values of M and N. Typical singular asymptotic expansions suggest that one should replace $\beta_0\tau$ by $\beta(\tau)$ and constant M by function $M(\tau)$. In considering a Taylor series expansion of $\beta(\tau)$, one can ignore the constant term (or alternatively, assume that it is grouped with the coefficient $M(\tau)$). Then the leading term of the Taylor series should be $\beta_0\tau$. This is what one obtains from the straight-forward expansion.

One method, the method of averaging, is appropriate for the Jeffcott equations since it begins with the assumption that

$$W = M(\tau) \exp(i\beta(\tau)) + N \exp(i\phi\tau).$$

Another method, multiple scales, is also appropriate because one can envision the action of the rotor being based on two different time scales. The results are identical for the two methods.

Instead of one time scale τ, assume the problem depends on many time scales:

$$T_0 = \tau, \; T_1 = \varepsilon\tau, \; T_2 = \varepsilon^2\tau, \; . \; . \; .$$

Henceforth, only T_0 and T_1 are used. Let $W(\tau) = W(T_0, T_1) = W_0(T_0, T_1) + \varepsilon W_1(T_0, T_1) + \; . \; . \; .$ Equation (9) becomes a partial differential equation since

$$d/d\tau = (\partial/\partial T_0)(dT_0/d\tau) + \varepsilon(\partial/\partial T_1)(dT_1/d\tau) = D_0 + \varepsilon D_1$$

and $(d^2/d\tau^2) = (D_0 + \varepsilon D_1)^2$.

Thus, one finds

$$(D_0 + \varepsilon D_1)^2(W_0 + \varepsilon W_1 + \; . \; . \; .) + C(D_0 + \varepsilon D_1)(W_0 + \varepsilon W_1 + \; . \; . \; .)$$
$$+ \kappa(W_0 + \varepsilon W_1 + \; . \; . \; .) = \varepsilon f(W_0 + \varepsilon W_1 + \; . \; . \; .) + E\phi^2 \exp(i\phi T_0). \qquad (10)$$

Equating like powers of ε yields

$$\varepsilon^0: \; D_0^2 W_0 + C D_0 W_0 + \kappa W_0 = E\phi^2 \exp(i\phi T_0). \qquad (11)$$

This is a linear problem with this steady-state solution

$$W_0 = M \exp(i\beta_0 T_0) + N \exp(i\phi T_0)$$

where $N = E\phi^2/(-\phi^2 + iC\phi + \kappa)$ and $M = M(T_1)$. To determine M one must examine the ε-order problem and choose M to eliminate secular terms; see Nayfeh [7]:

$$\varepsilon^1: \; D_0^2 W_1 + C W_1 + \kappa W_1 = -2D_0 D_1 W_0 - C D_1 W_0 + f(W_0).$$

With $V = k\Delta/\varepsilon$, the right-hand side of the last equation becomes

$$-2i\beta_0 M' \exp(i\beta_0 T_0) - CM' \exp(i\beta_0 T_0)$$
$$+ V(1/|W_0| - 1)\,[M \exp(i\beta_0 T_0) + N \exp(i\phi T_0)]$$

where $|W_0| = \{|M|^2 + |N|^2 + \bar{M}N \exp[i(\phi - \beta_0) T_0] + \bar{M}N \exp[i(\beta_0 - \phi)T_0]\}^{\frac{1}{2}}$. To aviod secular terms one requires that the collective coefficient of $\exp(i\beta_0 T_0)$ be zero. Although an anlytic solution of the differential equation for $M(T_1)$ has not been found, one can qualitatively assess M based on a similar problem (van der Pol's equation) and specific numerical results (presented below).

Since $M(T_1)$ is complex, it may be written as $M(T_1) = \rho(T_1) \exp[i\hat{\beta}(T_1)]$. Thus,

$$W_0 = \rho(T_1) \exp[i\beta_0 T_0 + i\hat{\beta}(T_1)] + N \exp(i\phi T_0)$$

or, assuming $\hat{\beta}(T_1)$ is analytic near $t = 0$, $W_0 = \rho(T_1) \exp[i(\beta_0 + \varepsilon\beta_1)\tau + \ldots]$ $+ N \exp(i\phi\tau)$. Thus the fundamental frequency of the nonlinear problem is not β_0 but $\beta = \beta_0 + \varepsilon\beta_1 + \ldots$; however, β must reduce to β_0 when $E\phi^2 = 0$. Consequently, the frequency $\gamma = \phi - \beta_0$ that appears in the expression for $|W_0|$ should be considered as $\gamma = \phi - \beta$. Then $1/|W_0|$ shows all frequencies $n\gamma$ and $W_0/|W_0|$ shows all frequencies $n\gamma \pm \beta$, for $n = 0, 1, \ldots$ This suggest that M has a complex Fourier series of the form:

$$\sum_{n=-\infty}^{\infty} s_n \exp(in\gamma T_1).$$

Another factor of M must also be included since numerical examples show that $M \equiv 0$ if $E\phi^2$ is greater than some fixed value. This is similar to the behavior of the van der Pol oscillator; see [7]. One possible form of M would include a factor of the form $F = 1/[1 + \exp(-\eta T_1)]$ where $\eta = \eta(E\phi^2)$. This would imply that $F \to 1$ as $\tau \to \infty$ when $\eta \geq 0$ and $F \to 0$ as $\tau \to \infty$ when $\eta < 0$. Thus, M looks like:

$$1/[1 + \exp(-\eta T_1)] \sum_{n=-\infty}^{\infty} s_n \exp(in\gamma T_1).$$

PSD plots of R show the frequencies $n\gamma$.

For the case of multiple forcing functions, $\sum_{i=1}^{L} F_i(\phi_i) \exp(i\phi_i \tau)$, one defines $\gamma_i = \phi_i - \beta$. Then the zeroth-order asymptotic approximation of the solution of equation (6) will contain L terms to account for the

L forcing frequencies, ϕ_i, i = 1, 2, . . ., L. Thus, the term N exp(iϕT_0) in W_0 is replaced by $N_1\exp(i\phi_1 T_0) + \ldots + N_L\exp(i\phi_L T_0)$. The coefficient M of the nonlinear frequency β will now contain the Fourier factor

$$\sum_{v} S_v \exp(i\gamma T_1)$$

where $\gamma = n_1\gamma_1 + \ldots + n_L\gamma_L$ and the summation is taken over the integer v from $-\infty$ to $+\infty$ with $v = n_1 + \ldots n_L$. Typical examples show significant magnitude coefficients, S_v, only for v = 0, +1, -1, +2, -2.

Figures 1 and 2 show typical numerical solutions which are obtained using Runge-Kutta fourth order on equations (1) and (2). The system constants used are these: $\mu = 0$, m = 1 lb. - s.^{2}/in., C_s = 240 lb. - s./in., K_s = 0., K_B = 1,305,000 lb./in., Q_s = 200,000 lb./in., δ = .0000285 in., and ω = 500 Hertz = 1000π rad./s. Thus, β_0 = 833.33 rad./s. and a = .000060915 in. The system is made nondimensional using a for the g-displacement and β_0 for the σ-frequency. With these choices, the constants of this equation

$$W'' + CW' + [k(1 - \Delta/|W|) - iB]W = E\phi^2\exp(i\phi\tau)$$

have these values: C = .288, k = 1.8792, Δ = .467865, B = .288, and ϕ = 6 /5.

Figures 1 and 2 show changes in the solution Y vs. Z as E assumes the values $100n/(1000\pi)^2$ a for n = 0, 1, . . ., 7. The graphs are plotted for .2 < t $\leq$ .5s. The initial circle (for E = 0) opens into an annular region, which becomes larger and thicker as E increases until a (transition) value of E occurs and the coefficient of exp(i$\beta\tau$) becomes zero. Thus, $W = N\exp(i\phi\tau)$, a circle of radius |N|. As E increases beyond this transition value, the solution remains a circle (Figure 2.d) with radius $|N| = |E\phi^2/(-\phi^2 + iC\phi + k(1 - \Delta/|N|) - iB)|$.

Figure 3, a typical full PSD plot, is the case $E = 4/10{,}000\pi^2 a$. As shown earler, one expects frequencies of ω and β to appear, as well as harmonics of $n\gamma\pm\beta$ where $\gamma = \omega - \beta$ and n = 1, 2, . . . Thus, with β = 150 Hertz, and ω = 500 Hertz, one predicts that the PSD plot will exhibit peaks at 150, 200, 500, 550, 850, 900, . . . Hertz. Figure 3 confirms these predictions.

3. CIRCLE OR ANNULUS

This section presents two theorems which provide analytic expressions that allow one to determine a priori whether a solution's geometry will be a circle or an annulus. Numerical examples are also included.

In this section we consider the Jeffcott equations without side force, viz.

$y'' + cy' + qy + Bz = F\cos\phi\tau$

$z'' + cz' - By + qz = F\sin\phi\tau$,

where $F = E\phi^2$, $r = (y^2 + z^2)^{\frac{1}{2}}$, $\phi > 0$, $E > 0$, $q = A + k(1 - \Delta r^{-1})$ if $r \geq \Delta$, and $q = A$ if $r < \Delta$. In polar form, and assuming that $r \geq \Delta$, we can write these equations as

$$w'' + cw' + \{A - iB + k - k\Delta/|w|\}w = E\phi^2 \exp(i\phi\tau). \tag{12}$$

Let $M = \dfrac{A + k - \phi^2}{B - \phi c}\,\phi^2$, and $F + M^2E^2 + \phi^4E^2 - k^2\Delta^2$.

We have:

Theorem 1. Assume $\phi c - B \neq 0$. Then the differential equation (12) has a solution of the form $w = r\exp(i\phi\tau + i\phi_0)$, $r \geq \Delta$, $\phi_0 \geq 0$, if and only if the following conditions are satisfied:

$$F \geq 0 \tag{13}$$

and either

$$k\Delta M + \phi^2(F)^{\frac{1}{2}} \leq E(M^2 + \phi^4) \tag{14}$$

and

$$\frac{(k\Delta M + \phi^2(F)^{\frac{1}{2}})\phi^2}{(M^2 + \phi^4)(B - \phi c)} \geq \Delta \tag{15}$$

or

$$|k\Delta M - \phi^2(F)^{\frac{1}{2}}| \leq E(M^2 + \phi^4) \tag{16}$$

and

$$\frac{(k\Delta M - \phi^2(F)^{\frac{1}{2}})\phi^2}{(M^2 + \phi^4)(B - \phi c)} \geq \Delta \tag{17}$$

If (13), (14) and (15) are satisfied, then, setting $v = \dfrac{k\Delta M + \phi^2(F)^{\frac{1}{2}}}{E(M^2 + \phi^4)}$, we have $\phi_0 = \arcsin v$ (18) and $r = E\phi^2 v/(B - \phi c)$ (19).

If (13), (16) and (17) are satisfied, then (18) and (19) hold with

$$v = \frac{k\Delta M - \phi^2(F)^{\frac{1}{2}}}{E(M^2 + \phi^4)}$$

Proof: Assume (12) has a solution of the form $w = r\exp(i\phi\tau + i\phi_0)$ with $r \geq \Delta$. Since $w' = i\phi w$ and $w'' = -\phi^2 w$, replacing in (12) we obtain $-\phi^2 r + i\phi rc + \{A - iB + k - k\Delta r^{-1}\} r = E\phi^2\exp(i\phi_0)$ Setting $u = \cos\phi_0$, $v = \sin\phi_0$, and separating real and imaginary parts, we obtain

$$(\phi c - B)r = -E\phi^2 v \tag{20}$$

and

$$-\phi^2 r + (A + k)r - k\Delta = E\phi^2 u, \text{ i.e.}$$

$$(A + k - \phi^2)r - k\Delta = E\phi^2 u \tag{21}$$

Case 1:

$$\phi c - B \neq 0$$

From (20) we know that $r = \dfrac{E\phi^2 v}{B - \phi c}$; (22)

whence from (21)

$$\frac{A + k - \phi^2}{B - \phi c} E\phi^2 v - k\Delta = E\phi^2\sqrt{1-v^2}.$$

Setting

$$M = \frac{A + k - \phi^2}{B - \phi c}\phi^2, \tag{23}$$

we have

$$MEv - k\Delta = E\phi^2\sqrt{1 - v^2}. \tag{24}$$

Squaring:

$$M^2E^2v^2 + k^2\Delta^2 - 2k\Delta MEv = E^2\phi^4 - E^2\phi^4v^2, \tag{25}$$

i.e.

$$(M^2 + \phi^4)\, E^2v^2 - 2k\Delta MEv + (k^2\Delta^2 - E^2\phi^4) = 0. \tag{26}$$

Setting

$$D = K^2\Delta^2M^2 - (M^2 + \phi^4)(k^2\Delta^2 - E^2\phi^4)$$

and

$$F = M^2E^2 + \phi^4E^2 - k^2\Delta^2 \tag{27}$$

we readily see that

$$D = \phi^4F,$$

$$Ev = \frac{k\Delta M \pm \phi^2\sqrt{F}}{M^2 + \phi^4}, \text{ i.e.}$$

$$v = E^{-1}\frac{k\Delta M + \phi^2\sqrt{F}}{M^2 + \phi^4} \tag{28}$$

or

$$v = E^{-1}\,(k\Delta M - \phi^2\sqrt{F})/(M^2 + \phi^4) \tag{29}$$

and therefore

$$F \geq 0. \tag{30}$$

Since $|v| \leq 1$, it is also clear that

either

$$k\Delta M + \phi^2\sqrt{F} \leq E(M^2 + \phi^4) \tag{31}$$

or

$$|k\Delta M - \phi^2\sqrt{F}| \leq E(M^2 + \phi^4). \tag{32}$$

Moreover, from (22) we know that

$$\frac{E\phi^2 v}{B - \phi c} \geq \Delta, \tag{33}$$

where v is given by (28) or (29).

Conversely, let M and F be defined by (23) and (27) respectively, and assume that (30), (33) and either (31) or (32) are satisfied. We claim that there is a solution of (12) of the form $w = r \exp(i\phi\tau + i\phi_0)$ with $r \geq \Delta$. To show this, assume for instance that (31) is satisfied, and let v be defined by (28).

Then

$$|v| \leq 1, \tag{34}$$

and v satisfies (26). Rearranging terms we obtain (25), whence taking the square root on both sides (24) follows. Let r be given by (22). Then clearly (20) is satisfied. Moreover, in view of (23) there is a $\phi_0 \geq 0$ such that $\sin\phi_0 = v$ and $\cos\phi_0 = \sqrt{1-v^2}$. Setting $u = \sqrt{1 - v^2}$, we see that (21) is satisfied. Moreover, from (33) we know that $r \geq \Delta$.

Setting

$w = r\exp[i\phi\tau + i\phi_0]$ the conclusion readily follows. Q. E. D.

Theorem 2. Assume $\phi c - B = 0$. Then the differential equation (12) has a solution of the form $w = r\exp(i\phi\tau + i\phi_0)$, $r \geq \Delta$, $\phi_0 \geq 0$, if and only if the following conditions are satisfied:

$$A + k - \phi^2 = 0 \tag{35}$$

or

$$A + k - \phi^2 \neq 0 \tag{36}$$

and either

$$\frac{E\phi^2 + k\Delta}{A + k - \phi^2} \geq \Delta \tag{37}$$

or

$$\frac{-E\phi^2 + k\Delta}{A + k - \phi^2} \geq \Delta. \tag{38}$$

Moreover:

(a) If (35) is satisfied then $r \geq \Delta$ is arbitrary, $\phi_0 = (2n + 1)\pi$, $n = 0, 1, 2, \ldots$, and $k\Delta = E\phi^2$

(b) If (36) and (37) are satisfied then $r = \dfrac{E\phi^2 + k\Delta}{A + k - \phi^2}$ and $\phi_0 = n\pi$, $n = 0, 1, 2, \ldots$,

(c) If (36) and (38) are satisfied then $r = \dfrac{-E\phi^2 + k\Delta}{A + k - \phi^2}$ and $\phi_0 = n\pi$, $n = 0, 1, 2, \ldots$

Proof:

Since $\phi c - B = 0$, (20) implies that $v = 0$, and therefore $u = \pm 1$. If (35) is satisfied, we conclude from (21) that $k\Delta = E\phi^2$ and $u = -1$. Thus $\phi_0 = (2n + 1)\pi$, $n = 0, 1, 2, \ldots$ and r is arbitrary. Conversely, assume that (35) is satisfied,

$$w = r\exp(i\phi\tau + (2n + 1)\pi i), \tag{39}$$

and $k\Delta = E\phi^2$. Then we readily conclude that (20) and (21) are satisfied, and therefore that (39) is a solution of (12).

Assume now that (36) is satisfied. Then (21) yields

$$r = \frac{E\phi^2 + k\Delta}{A + k - \phi^2} \tag{40}$$

provided that (37) holds, or

$$r = \frac{-E\phi^2 + k\Delta}{A + k - \phi^2}, \tag{41}$$

provided that (38) holds. Moreover, it is clear that $\phi_0 = n\pi$, $n = 0, 1, 2, \ldots$

Conversely, assume that (36) is satisfied, and let r be given by (40) (if (37) holds), or by (41) (if (38) holds), and let $\phi_0 = n\pi$, $n = 0, 1, 2, \ldots$ We then readily see that (20) and (21) are satisfied, and therefore that $w = r\exp(i\phi\tau + in\pi)$ $(n = 0, 1, 2, \ldots)$ is a solution of (12). Q. E. D.

Numerical examples are now presented to illustrate the results of these theorems. Consider these given parameters:

$m = 1$

$K_s = 0$

$K_B = 1{,}305{,}000$

$Q_s = 200{,}000$

$C_s = 240$

$u = .0000285$

$\delta = .00000285$

and use the nondimensionalizing frequency $\sigma = \sqrt{(K_s + K_B)}$ and the nondimensionalizing displacement $g = u$. Table 1 summarizes a frequency-response curve as ϕ, the nondimensional forcing frequency, varies from 0.0 to 2.0 in increments of 0.1. The corresponding values of R are obtained from the Runge-Kutta solutions. From Table 1 one sees that the solution is a circle for all values of ϕ except $\phi = 0.1$. Generally speaking, one expects the solution to be an annulus over an interval of ϕ, not just at one point. The theorems, however, can find this interval in much less (computer) time and show that the solution is an annulus for $0 < \phi < 0.11$.

Table 2 uses the same parameters as Table 1 except that $\delta = .0000285$; i.e., $\delta = u$ instead of $\delta = .1u$ (in Table 1). In this case an annulus appears for $\phi = .1, .2, .3$ and for $\phi = 1.0$ to 2.0. Figures 4, 5, and 6 are the Runge-Kutta solutions for $\phi = .3, .9$, and 1.5, respectively. From the theorems one has that the solution is an annulus for $0 < \phi \leq .31$ and for $1.0 \leq \phi \leq 2.0$.

Table 3 changes only the δ in Tables 1 and 2 to $\delta = 10u$. The theorem delimits the ϕ-intervals for an annulus to be $0 \leq \phi \leq .61$ and $.84 \leq \phi \leq 2.0$.

These examples lead one to abandon repeatedly plotting Runge-Kutta solutions in order to determine intervals of annuli. Rather, one employs the inequalities of the theorems to determine these intervals thereby allowing one's focus to shift to variations in the ratio δ/u.

Table 4 summarizes seven such ratios for the same data of Tables 1, 2, and 3. The three cases, $\delta/u = 0.1$, 1.0, and 10.0 of the preceeding Tables, are included here along with four other values, $\delta/u = 0.5$, 0.9, 2.0, and 5.0, to give a smoother picture of how the frequency-response curves depend on this ratio. One should bear in mind that each description

(listed as "circle/annulus regions") for a fixed δ/u ratio is itself a frequency-response curve. The most interesting feature seen by comparing these seven curves is that there is only one transition point, from annulus to circle, in the curves for $\delta/u < 1.0$ (excluding the initial circle at $\phi = 0$). But for $\delta/u \geq 1.0$ there is a transition point from annulus to circle and another transition point from circle back to annulus.

Figure 7 is the frequency response curve of Table 4 with $\delta = u$. The regions where the response is an annulus are shown in the figure with the outer radius of the annulus only.

Tables 5 and 6 are the same as Table 4 except that the bearing stiffness, K_B, is changed. Table 5 uses $K_B = 700{,}000$, a value that is close to an unstable solution. Table 6 uses $K_B = 10{,}000{,}000$, a very stiff bearing. These tables are included to illustrate that the frequency-response curves of Table 4 are not atypical.

4. ROTORS WITH MASS IMBALANCE AND SIDE FORCE

Thus far, the analysis has concentrated on the Jeffcott equations containing only one forcing function, which is mass imbalance in the numerical examples, but can be any sinusoidal force, $F \exp(i\omega t)$.

We begin our initial investigation into multiple forcing functions by examining the most improtant case in applications, viz., mass imbalance plus side force. The side force appears in the Jeffcott equations as a constant in the y-direction only. In general, one has the following nondimensional, complex form of the Jeffcott equations with side force and mass imbalance:

$$W'' + CW' + (A + k(1 - \Delta/R) - iB)\, W = S + E\phi^2 \exp(i\phi\tau)$$

where $W = Y + iZ$. If the dimensional side force is, Sf, then the nondimensional side force is $S = Sf/mass/\sigma^2/g$.

In the corresponding linear problem ($\Delta = 0$), one finds the solution to be the sum of two parts: (i.) a constant, resulting from the side force S and (ii.) a sinusoidal, resulting from the mass imbalance. Said another way, the solution of the linear problem is a sinusoidal shifted by a constant (the side force contribution).

In an analogous manner, one predicts the addition of side force to the nonlinear problem will cause a constant shift in the solution of the nonlinear problem without side force. There are, however, slight modifications that must be made since one is dealing with a nonlinear problem and the principle of superposition no longer holds exactly. For example, a circle or circular annulus will be changed into an ellipse or an elliptical annulus, but otherwise no fundamentally different curves should appear.

Upon examining the numerous results of the Control Dynamics Company Report [3], one sees that this is the case; i.e., regardless of whether one has A-motion, B-motion, or C-motion, the trajectory of the solution of the Jeffcott equations is a shifted ellipse or a shifted elliptical annulus.

Detailed results of the CDC Report [7] are now considered.

CDC-Figure 2.3a: A-motion within deadband. In this case (within deadband), the Jeffcott equations are linear and the trajectory is a circle

that has been shifted from the origin by a fixed amount in the y and z directions. This is exactly as expected. Note that the solution shifts in both the y and z directions even though the Jeffcott equations contain a side force in the y direction only. This is caused by the coupling of the two equations. Figures 8 and 9 reproduce these results.

CDC-Figure 2.4a: A-motion overlapping deadband. Now the shifted circle becomes a shifted ellipse since the motion includes the nonlinear region outside the deadband. Still this is what is expected. Figures 10 and 11 reproduce these results.

CDC-Figure 2.5a: A-motion outside deadband. Again a shifted ellipse.

CDC-Figure 2.6a: A-motion outside deadband. Again a shifted ellipse.

CDC-Figure 2.7a: A-motion overlapping deadband. Again a shifted ellipse. Figures 12 and 13 reproduce these results.

CDC-Figure 2.8a: A-motion overlapping deadband. Again a shifted ellipse.

CDC-Figure 2.9a: B-motion overlapping deadband. A shifted elliptical annulus. The earlier investigators apparently labeled the annular regions observed from numerical results as B-motion. It is now understood that this "erratic" motion is actually an annulus and is caused by including contributions from the left-hand side of the Jeffcott equations (the homogeneous solution). If the side force (causing a shift of the center) were omitted, a circular, annular orbit would result. In the corresponding PSD plot of CDC-Figure 2.9b, one sees the subsyncronous frequency appear at half the driving frequency. This is no surprise since the damping and cross-coupling ratio was chosen to be exactly one half the driving frequency. Figures 14 and 15 reproduce these results.

CDC-Figure 2.10a: B-motion surrounding the origin and overlapping deadband. Again a shifted elliptical annulus. The "radius" of the resulting elliptical annulus appears to be a direct result of the mass imbalance, whereas the center of the elliptical annulus is caused by the side force. Therefore, in this case the center is close to the origin in comparison with the "radius" of the elliptical annulus. This suggests that the mass imbalance is much larger than the side force for this case. Indeed, according to the key, this is the case of the largest mass imbalance and the second smallest side force considered.

CDC-Figure 2.11a: B-motion surrounding deadband. Again an elliptical annulus.

CDC-Figure 2.12a: C-motion surrounding deadband. The original investigators defined C-motion to be a shifted elliptic annulus motion that completely surrounds the deadband. By our analysis there is no need to distinguish between B-motion and C-motion. The two are resulting from the same analytic case: motion caused by side force, mass imbalance and a contribution from the homogeneous equation. It is A-motion, where there is no contribution from the homogeneous equation that is different. A-motion is a shifted ellipse, whereas B-motion and C-motion are shifted elliptical annuli. This is further verified by examining the PSDs of the B-motions and C-motions. In B- or C-motion one sees a peak occuring at the subsynchronous frequency which is exactly half the driving frequency.

CDC-Figure 2.13a: C-motion surrounding deadband. Again a shifted elliptical annulus. Here the thickness of the annulus is so small that it is hard to see in the graph. But one can see that it is actually there by examining the corresponding PSD. Also from the PSD one sees that the major contribution is at the subsynchronous frequency rather than the driving frequency. This is because of the comparative sizes of the three parameters.

CDC-Figure 2.14a: C-motion touching deadband. Again a shifted elliptical annulus. It is really B-motion. The thickness of the annulus in minute compared with its "radius". Figures 16 and 17 reproduce these results.

5. MULTIPLE EXCITATIONS

In this section the generalized, complex Jeffcott equation (6) is considered. The examples deal with the case L = 2 in equation (6); i.e., the nonlinear Jeffcott equation is being forced by two functions, $F_1 \exp(i\phi_1\tau)$ and $F_2 \exp(i\phi_2\tau)$.

Define $\gamma_1 = \phi_1 - \beta$ and $\gamma_2 = \phi_2 - \beta$ where ϕ_1 and ϕ_2 are the two forcing frequencies and β, as in the case of the single forcing function, is the nonlinear frequency resulting from the homogeneous portion of the Jeffcott equation; i.e., $\beta = \beta_0 + \varepsilon\beta_1 + \ldots$.

Certainly one expects to see the frequencies ϕ_1 and ϕ_2 in the response's PSD. But also one sees all frequencies $|\gamma \pm\beta|$ where $\gamma = n_1\gamma_1 + n_2\gamma_2$ and $n_1 + n_2 = v$ with integer v ranging from $-\infty$ to $+\infty$. Thus, for $v = 0$, $n_1 + n_2 = 0$ and as ordered pairs $(n_1, n_2) = (0, 0), (1, -1), (-1, 1), (2, -2), (-2, 2), \ldots$. Hence, $v = 0$ corresponds to $\gamma = 0, |\phi_1 - \phi_2|, 2|\phi_1 - \phi_2|, 3|\phi_1 - \phi_2|, \ldots$. For $v = 1$, $(n_1, n_2) = (0, 1), (1, 0), (-1, 2), (2, -1), (-2, 3), (3, -2), \ldots$ and correspondingly $\gamma = \phi_2-\beta, \phi_1 -\beta, 2\phi_2 - \phi_1 -\beta, 3\phi_2 - 2\phi_1 - \beta, 3\phi_1 - 2\phi_2 -\beta, \ldots$. As in the single forcing function case, many of these frequencies may not appear in the solution's PSD, depending upon the relative magnitudes of the coefficients of the homogeneous equation and the forcing magnitudes F_1 and F_2.

Considered now are three examples which use the same homogeneous coefficients as the example in Subsection 2.4; i.e., $m = 1$, $C_s = 240$, $K_s = 0$, $K_B = 1{,}305{,}000$, $Q_s = 200{,}000$ and $\delta = 0.0000285$. Again $\beta_0 = 833.3$ and $\beta = \beta_0+ \varepsilon\beta_1 + \ldots$.

The first example uses $F_1 = 50$, $\phi_1 = 300$ Hz., $F_2 = 350$ and $\phi_2 = 500$ Hz. The response is shown in Figure 18 and the corresponding PSD of y appears in Figure 19. The three largest peaks occur at 155 Hz., 300 Hz., and 500 Hz. Certainly, the last two are no surprise. Likewise, the 155 Hz. peak is again corresponding to the β, the homogeneous solution. Secondary peaks at 60 Hz. and 220 Hz. can be accounted for with

$$3\gamma_1 - 8\gamma_2 + \beta = 3(340) - 8(140) + 160 = 60$$

$$\gamma_1 - 2\gamma_2 + \beta = 340 - 2(140) = 220.$$

Minor peaks at 20 Hz., 340 Hz., 360 Hz. and 420 Hz. can also be included since

$0(\gamma_1) - \gamma_2 + \beta = -140 + 160 = 20$

$3(\gamma_1) - 6(\gamma_2) + \beta = 3(340) - 6(140) + 160 = 340$

$\gamma_1 - \gamma_2 + \beta = 340 - 140 + 160 = 360$

$2\gamma_1 - 3\gamma_2 + \beta = 2(340) - 3(140) + 160 = 420.$

The second example replaces F_1 and F_2 of the previous exercise with $F_1 = 200 = F_2$. Again $\phi_1 = 300$ Hz. and $\phi_2 = 500$ Hz. Figures 20 and 21 display the solution and its PSD, respectively. The PSD exhibits only the peak, at 100 Hz., other than the mandatory peaks at 300 Hz. and 500 Hz. But this can be accounted for as $2(300) - 500$, or with $\beta = 150$ Hz., one has

$-\gamma_1 + 2\gamma_2 + \beta = -350 + 2(150) + 150 = 100.$

Finally, the replacement of F_1 with 350 and F_2 with 50 leads to the solution which is drawn in Figure 22 and to its associated PSD in Figure 23. The explanation of this example is analagous to the previous example.

6. STABILITY

This Section contains two theorems, one related to the critical points of a first order system of dimension six and the other related to bounds of the solution of the same system. The Section concludes with examples of bounded and unbounded solutions, which occur in corresponding regions of the linear problem.

In this section we consider the Jeffcott equations with side force, viz.

$$\begin{aligned} y'' + Cy' + qy + Bz &= F\cos\phi\tau + D \\ z'' + Cz' - By + qz &= F\sin\phi\tau, \end{aligned} \tag{42}$$

where $F = E\phi^2$, $r = (y^2 + z^2)^{\frac{1}{2}}$ and $q = A + k(1 - \Delta r^{-1})$ if $r \geq \Delta$, and $q = A$ if $r < \Delta$. We start with

Theorem 1. Let $u_1 = y$, $u_2 = y'$, $u_3 = y''$, $u_4 = z$, $u_5 = z'$, $u_6 = z''$, $M = [F^2 - (u_3 + Cu_2 + qu_1 + Bu_4 - D)^2]^{\frac{1}{2}}$, and $N = [F^2 - (u_6 + Cu_5 - Bu_1 + qu_4)^2]^{\frac{1}{2}}$.

Then every solution of (42) is a solution of the autonomous system

$$\begin{aligned} u_1' &= u_2 \\ u_2' &= u_3 \\ u_3' &= -q'u_1 - qu_2 - Cu_3 - Bu_5 - M\phi \\ u_4' &= u_5 \\ u_5' &= u_6 \\ u_6' &= Bu_2 - q'u_4 - qu_5 - Cu_6 + N\phi \end{aligned} \tag{43}$$

Moreover, no solution of (42) passes through a critical point of (43).

Proof From the first of the equations (42) we have $\cos\phi\tau = (y'' + Cy' + qy + Bz - D)/F$. Thus $\phi\tau = \text{Arccos}[(y'' + Cy' + qy + Bz - D)/F]$. Differentiating we see that

$$\phi = -[F - (y'' + Cy' + qy + Bz)^2]^{-\frac{1}{2}} [y''' + cy'' + qy' + Bz' + q'y],$$

or

$$\phi = -M^{-1} (u_3' + Cu_3 + qu_2 + q'u_1 + Bu_5), \text{ whence}$$

$$u_3' = -q'u_1 - qu_2 - Cu_3 - Bu_5 - M\phi. \tag{44}$$

Similarly, from the second of the equations of (42) we see that $\sin\phi\tau = (z'' + Cz' - By + qz)/F$, or $\phi\tau = \text{Arcsin}[(z'' + Cz' - By + qz)/F]$, whence we readily conclude that

$$u_6' = Bu_2 - q'u_4 - qu_5 - Cu_6 + N\phi. \tag{45}$$

Combining (44), (45), and the definition of the variables u_i, (43) readily follows. We now turn our attention to the critical points. By definition,

$$u_2 = u_3 = u_5 = u_6 = 0, \text{ and therefore } -q'u_1 - M\phi = 0, \text{ and } -q'u_4 + N\phi = 0. \tag{46}$$

Assume the pair (u_1, u_4) is a solution of (42) (i.e. $u_1 = y$, $u_4 = z$).

In view of the definitions of M and N, we readily conclude that $M = F|\cos\phi t|$ and $N = F|\sin\phi t|$. Assume $r < \Delta$; then $q' = 0$, and from (46) we infer that $M = N = 0$. Since $M^2 + N^2 = F^2 \neq 0$, we have a contradiction. Assume now that $r \geq \Delta$. Then $q' = k\Delta R^{-2}R'$. Since $r = (y^2 + z^2)^{\frac{1}{2}}$, $r' = (y^2 + z^2)^{-\frac{1}{2}}(yy' + zz')$. Since $y' = u_2 = 0$, and $z' = u_5 = 0$, we conclude that $r' = 0$, and therefore $q' = 0$, and we have a contradiction, as in the first case. Q. E. D.

$\rho = 0$ if $|W| < \Delta$ and $\rho = 1$ if $|W| \geq \Delta$. Then the Jeffcott equations are equivalent to

$$W'' + CW' + (A - iB)W + k\rho W(1 - \Delta/|W|) = F\exp(i\phi t) + D, \tag{47}$$

where $W = y + iz$. We have:

Theorem 2. Let $\exp(\lambda t)$ be a solution of

$v'' + Cv' + (A\ iB + k)v = 0$, let $\lambda = a + ib$,

and assume that

$|W| > \Delta$ if $t_0 < t < t_1 \leq \infty$.

Then there exist constants M_1, M_2, M_3 such that if

$t_0 < t < t_1$, $|W| \leq M_1 + M_2 \exp(at) + M_3 \exp[-(a + c)t]$.

In particular if $-c \leq a \leq 0$, W will be bounded thereon.

Proof of Theorem 2: Let $G = A - iB + k\rho$. Then (47) can be written as

$$W'' + CW' + GW - \rho kW/|W| = F\exp(i\phi t) + D. \tag{48}$$

Let $W = uv$, where $v'' + cv' + Gv = 0$. Then (48) is transformed into

$u''v + 2u'v' + uv'' + cu'v + cuv' + Guv - \rho kW/|W| = F\exp(i\phi t) + D$, i.e.

$$u''v + (2v' + cv)u' - \rho kW/|W| = F\exp(i\phi t) + D. \tag{49}$$

Assume $v = \exp(\lambda t)$ and $\lambda = a + ib$; then (49) becomes

$u'' + (2\lambda + c)\,u' - \rho k(u/|u|)\exp(-\lambda + ib)t$

$= F\exp(i\phi - \lambda)t + D\exp(-\lambda t)$

Multiplying by $\exp(2\lambda + c)t$ we have

$[u'\exp(2\lambda + c)t]' - \rho k(u/|u|)\exp(\lambda + c + ib)t$

$= F\exp(i\phi + \lambda + c)t + D\exp(\lambda + c)t.$

Assume $|W| \geq \Delta$ if $t \geq t_0$. Integrating, we have

$u'\exp(2\lambda + c)t =$

$$k\int_{t_0}^{t}(u/|u|)\exp(\lambda + c + ib)s\,ds + [F/(i\phi + \lambda + c)][\exp(i\phi + \lambda + c)t - \exp(i\phi + \lambda + c)t_0] + [D/(\lambda + c)][\exp(\lambda + c)t - \exp(\lambda + c)t_0] + u'(t_0)\exp(2\lambda + c)\,t_0.$$

Multiplying by $\exp[-(2\lambda + c)t]$ we obtain:

$u' = k \exp[-(2\lambda + c)t] \int_{t_0}^{t} (u/|u|) \exp(\lambda + c + ib)s\,ds + [F/(i\phi + \lambda + c)]$

$\exp(i\phi - \lambda)t + [D/(\lambda + c)] \exp(-\lambda t) + E \exp[-(2\lambda + c)t].$

Thus,

$|u'| \leq k \exp[-2a + c)t] \int_{t_0}^{t} \exp(a + c)s\,ds + |F/(i\phi + \lambda + c)| \exp(-at) +$

$|D/(\lambda + c)| \exp(-at) + |E| \exp[-(2a + c)t] \leq$

$K_1 \exp(-at) + K_2 \exp[-(2a + c)t].$

Integrating, we conclude that

$|u| \leq k_3 \exp(-at) + K_4 \exp[-(2a + c)t] + k_5$. Thus,

$|W| = |u \exp(\lambda t)| \leq K_3 + K_4 [-(a + c)t] + K_5 \exp(at),$

whence the conclusion follows. Q. E. D.

Remark: From Theorem 2 we deduce that if $-c \leq a \leq 0$, then no solution of the Jeffcott equations can diverge to infinity. This does not preclude, however, the possibility of unbounded oscillatory behavior, $|W|$ could behave like, for example, $|\sin t| \exp(t)$, as t goes to infinity. The reason for this is that, if $|W| < \Delta$ for some interval (t_1, t_2) (with $t_1 > t_0$), and $|W| \geq \Delta$ for $t \geq t_2$, then for $t > t_2$ the constants M_1, M_2, and M_3 will depend on $W(t_2)$ and $W'(t_2)$.

As shown in Subsection 2.3 the eigenvalues of the linear Jeffcott equations ($\delta = 0$) corresponding to equations (1) and (2) are these:

$$\lambda = -C_s/2 \pm \sqrt{(C_s/2)^2 - (K_s + K_B) \pm iQ_s}.$$

Hence, the solutions are bounded if and only if $\mathrm{Re}(\lambda) < 0$; i.e.,

$$\mathrm{Re}[\sqrt{(C_s/2)^2 - (K_s + K_B) \pm iQ_s}] < C_s/2.$$

A similar result is obtained by considering the linear portion of the six first-order equations of system (43).

Table 7 is a listing of values where $\lambda = 0$ for $C_s = 150$ and $C_s = 240$. These values are shown graphically in Figure 24 together with $C_s = 100$ and $C_s = 300$. In all four cases the linear solution is bounded if the corresponding choices for $K_s + K_B$ and Q_s lie above the curve in question and unbounded below the curve.

This Section concludes with four examples of the nonlinear Jeffcott equation. Figure 25 is the solution of equations (1) and (2) with $C_s = 240$, $Q_s = 200{,}000$, $K_s = 0$, $K_B = 650{,}000$, $\omega = 500$ Hz., $\delta = .0000285$, and $u = 400/\omega^2$. From Figure 24 this solution is unbounded which agrees with Figure 25.

The second example is the same as the previous example except that K_B = 750,000. The corresponding linear solution (δ = 0) from Figure 24 is bounded. Figure 26 draws this solution.

The last two examples change only C_s to 150 and K_B to 3,500,000 and 4,500,000 respectively. From Figure 24 the smaller K_B value will produce an unbounded linear solution while the latter K_B value will produce a bounded linear solution. Figures 27 and 28 verify these results for the nonlinear problems.

7. CONCLUSIONS

This report has developed new theory and examples for the nonlinear Jeffcott equations in an attempt to offer mathematical explanations to observed phenomena. The emphasis here has been on constructing an understanding of vibrations induced in rotors by nonlinearities in the governing differential equations.

To this end, a review of the analysis of a single forcing function driving the Jeffcott equations lead directly to an examination of multiple forcing functions, in particular those which are caused by mass imbalance, side force, and rubbing. The theory presented herein is a generalization of all three of these specific forces and works well for any number of forcing functions.

As was shown in Final Report [4], a nonlinear frequency induced by the homogeneous portion of the Jeffcott equations appears in the PSD of the solution and is a basis for harmonics, formed by the difference between it and the forcing frequency, also to arise. In the case of two or more forcing functions, this nonlinear frequency again surfaces, along with a multitude of harmonics which are composed of sums and differences of the nonlinear frequency and each of the forcing frequencies. Examples in this report illustrate this analytic result for the specific case of mass imbalance and side force as well as the general case of any two forcing frequencies.

It was also shown in [4] that the nonlinear frequency is an elusive quantity in the sense that for some particular problems it is part of the PSD of the solution while in other problems it is absent. Therefore, one of the primary goals of this work has been to try to determine a priori for a given set of constants if the nonlinear frequency would actually be a part of the solution's PSD. Section 3 of this report presented a set of inequalities, based solely on the coefficients of the Jeffcott equations, which can make this decision.

The stability problem has continued to resistant analytic expression. Even though the Jeffcott equations were successfully transformed into a set of autonomous, first-order differential equation for which volumes of stability theory exist, it was also shown that the critical points of this

system, which are the basis of any stability analysis, do not lie within a region of the y-z plane which is physically interesting. Therefore, it was necessary to deal only with boundedness results of the solution. Some new results for bounded solutions were displayed, and these lead one to consider trying to prove the conjecture analytically that the effect of deadband on stability is that of stabilizing. This is seen immediately in the Jeffcott equations themselves where the only nonlinearity occurs in the form $1 - \delta/r$ so that if a solution attempts to grow without bound (r becomes infinite), then the nonlinearity approaches one and the problem becomes linear. This is again a boundedness result, but it does hint at stabilization.

One of the most interesting features of this fascinating problem has to date not been considered. That is this: how is the solution affected by variations in the initial conditions? Throughout the examples in this Report and in the previous Final Report [4], the initial conditions were never changed. It was only in making comparisons of the theory presented herein with the results of the Control Dynamics Company [3] that differences in solutions was observed for different initial conditions. While it is well-known in elementary theory of differential equations, that a change in the initial conditions of a nonlinear differential equation can have profound effects on the equation's solution, the Jeffcott equations behave so much like linear equations in a global sense that this idea of varying the initial conditions had never occurred. It is believed that this behavior affects whether the nonlinear frequency appears in a particular solution, but not that a nonlinear frequency exists. Thus, the fundamental results of this Report are not invalid, but rather another aspect of the problem should be examined.

8. REFERENCES:

1. Childs, D. W., "The Space Shuttle Main Engine High-Pressure Fuel Turbopump Rotordynamics Instability Problem", Trans. ASME, Journal of Engineering for Power, Jan. 1978, pp. 48 - 57.

2. Childs, D. W., "Rotordynamic Characteristics of the HPOTP (High Pressure Oxygen Turbopump) of the SSME (Space Shuttle Main Engine)", NASA MSFC Contract NAS8-34505, Turbomachinery Laboratories Report RD-1-84, 30 January 1984.

3. Control Dynamics Company, "Effects of Bearing Deadbands on Bearing Loads and Rotor Instability", NASA MSFC Contract NAS8-35050, 20 January 1984.

4. Day, W. B., "Nonlinear Rotordynamics Analysis", NASA MSFC Contract NAS8-35992, 15 March 1985.

5. Gupta, P. K., Winn, L. W., and Wilcock, D. F., "Vibrational Characteristics of Ball Bearings", Journal of Lubrication Technology, ASME Trans., Vol 99F, No. 2, 1977, pp. 284 - 289.

6. Jeffcott, H. H., "The Lateral Vibration of Loaded Shafts in the Neighborhood of a Whirling Speed - The Effect of Want of Balance", Philosophical Magazine, Series 6, Vol 37, 1919, p. 304.

7. Nayfeh, A. H., Perturbation Methods, J. Wiley & Sons, 1973.

8. Yamamoto, T. T., "On Critical Speeds of a Shaft", Memories of the Faculty of Engineering, Nagoya (Japan) University, Vol. 6, No. 2, 1954.

Figure 1

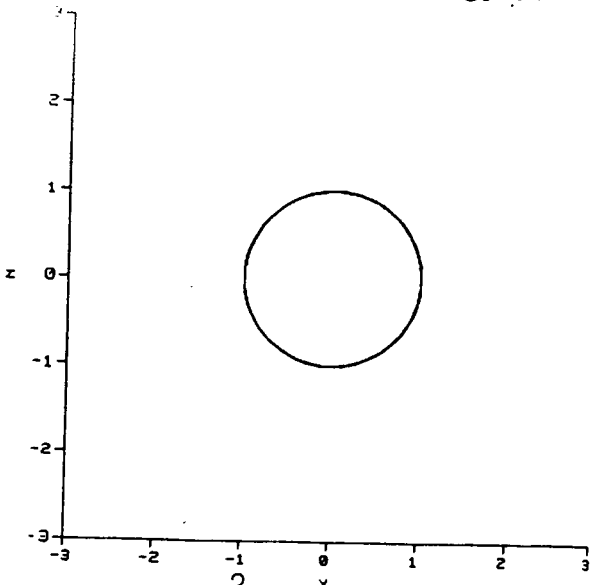

(a.) $u\omega^2 = 0$

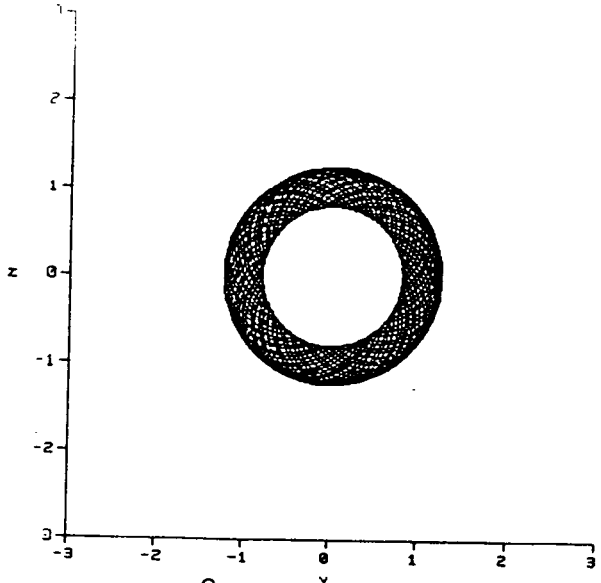

(b.) $u\omega^2 = 100$

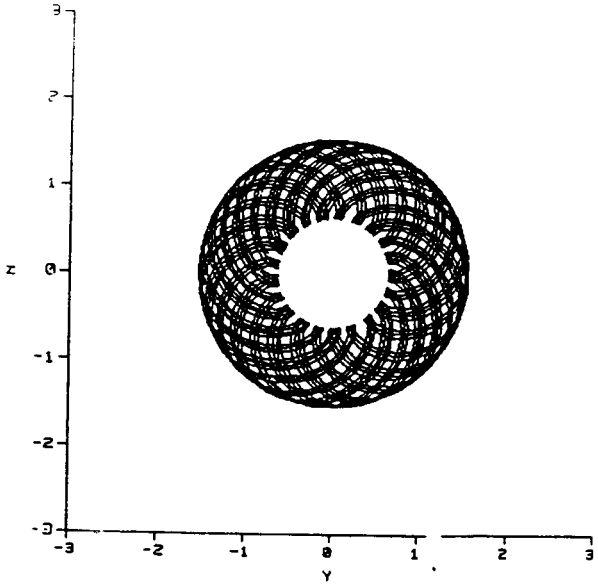

(c.) $u\omega^2 = 200$

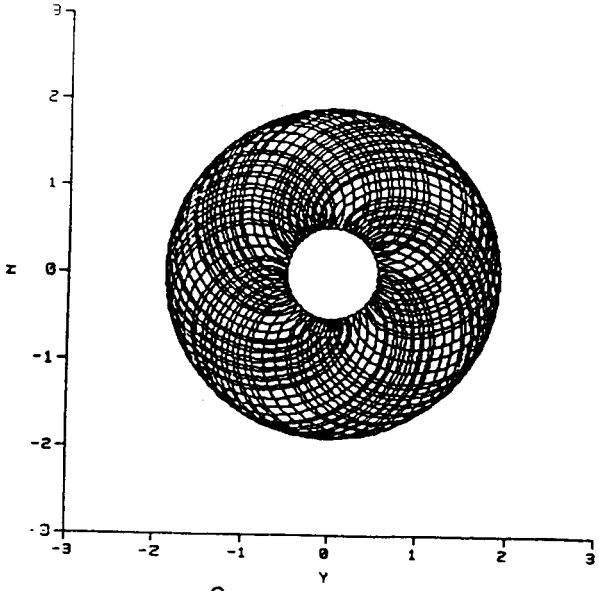

(d.) $u\omega^2 = 300$

Figure 2

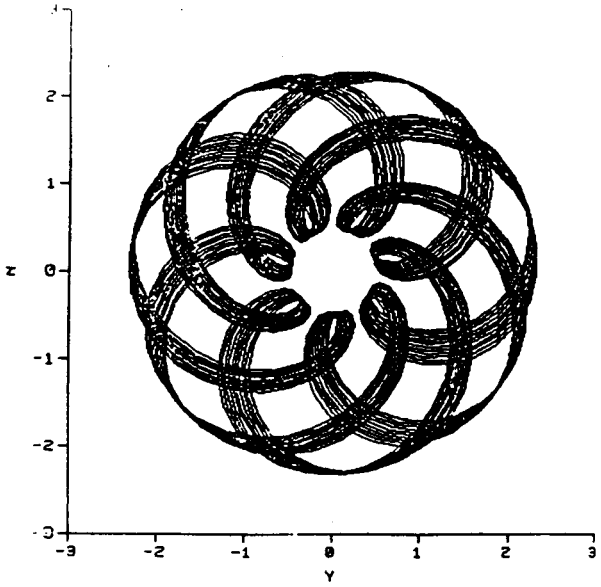

(a.) $u\omega^2 = 400$

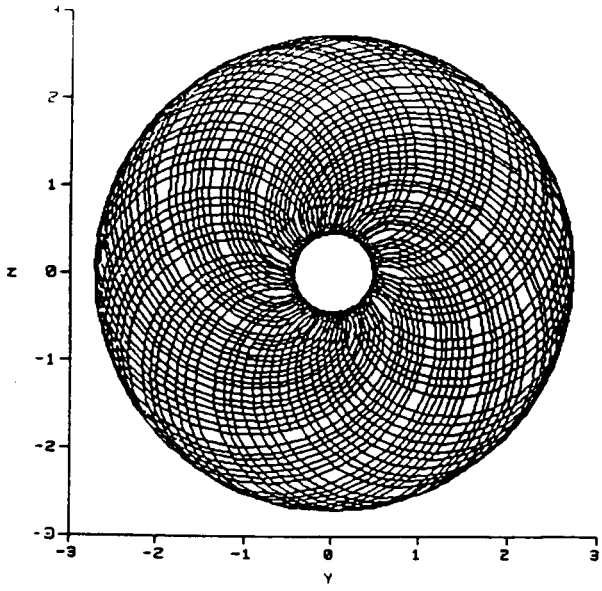

(b.) $u\omega^2 = 500$

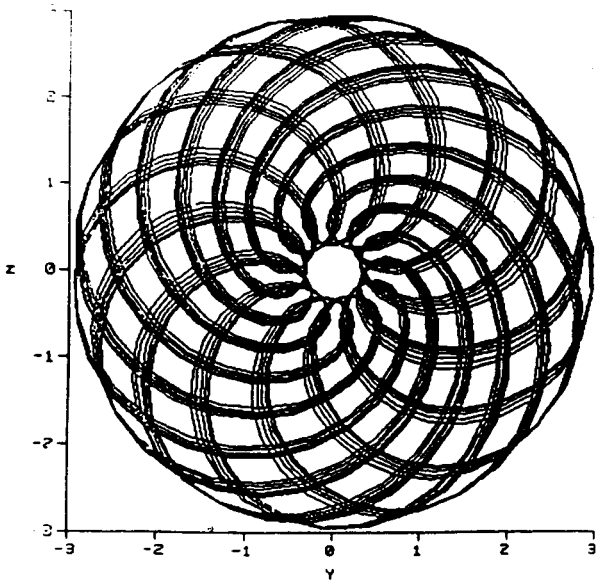

(c.) $u\omega^2 = 600$

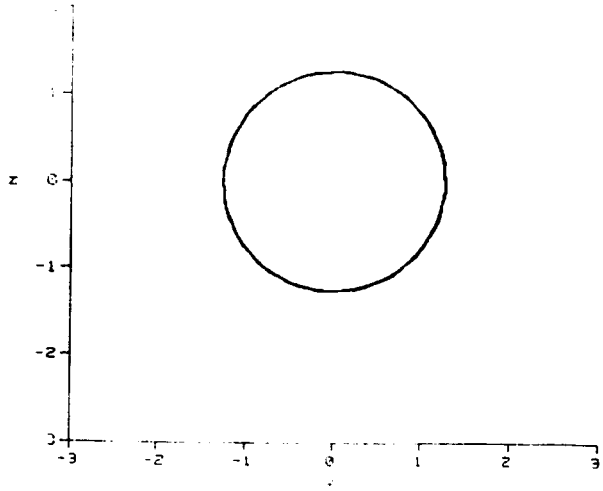

(d.) $u\omega^2 = 700$

Figure 3

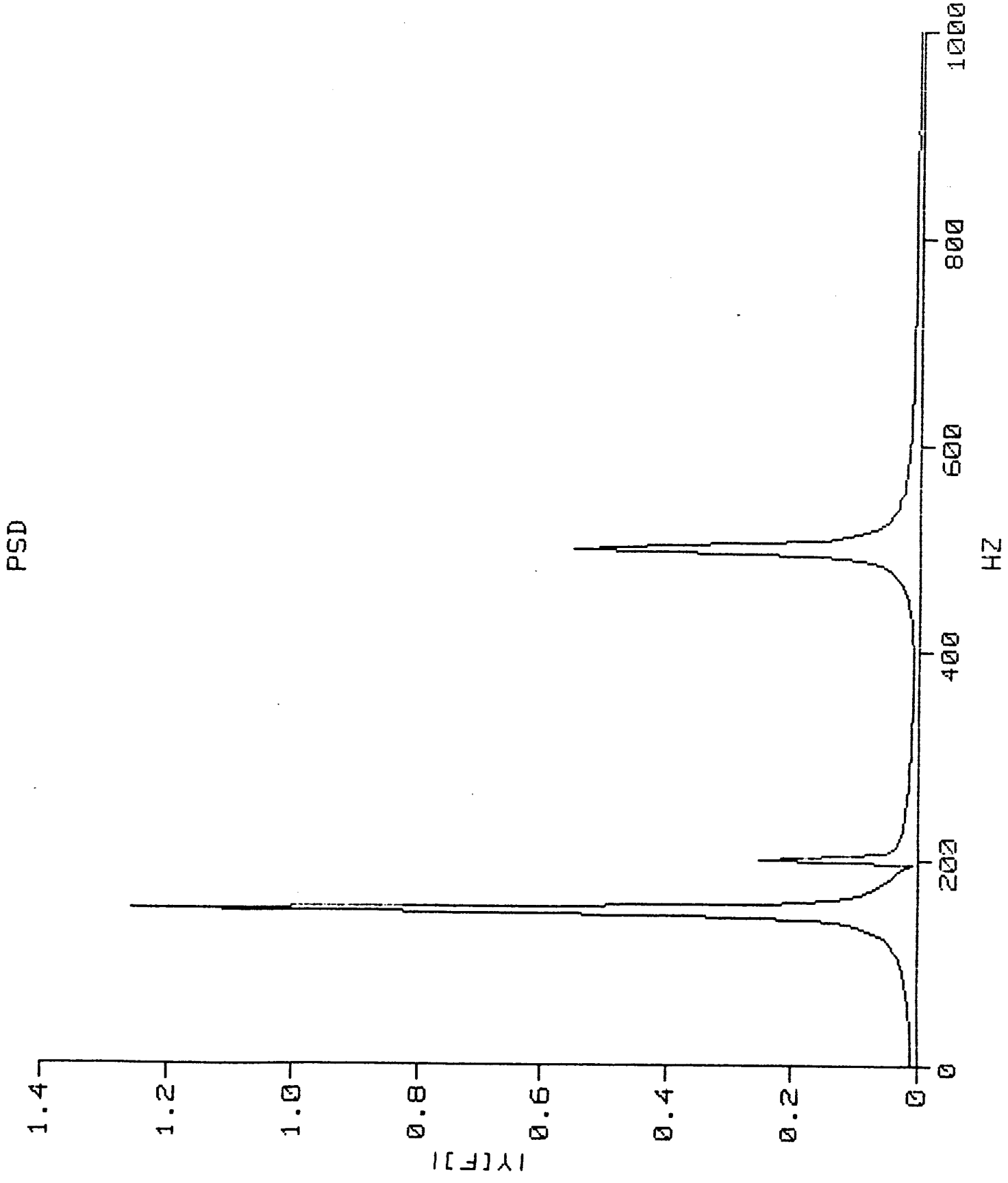

Figure 4

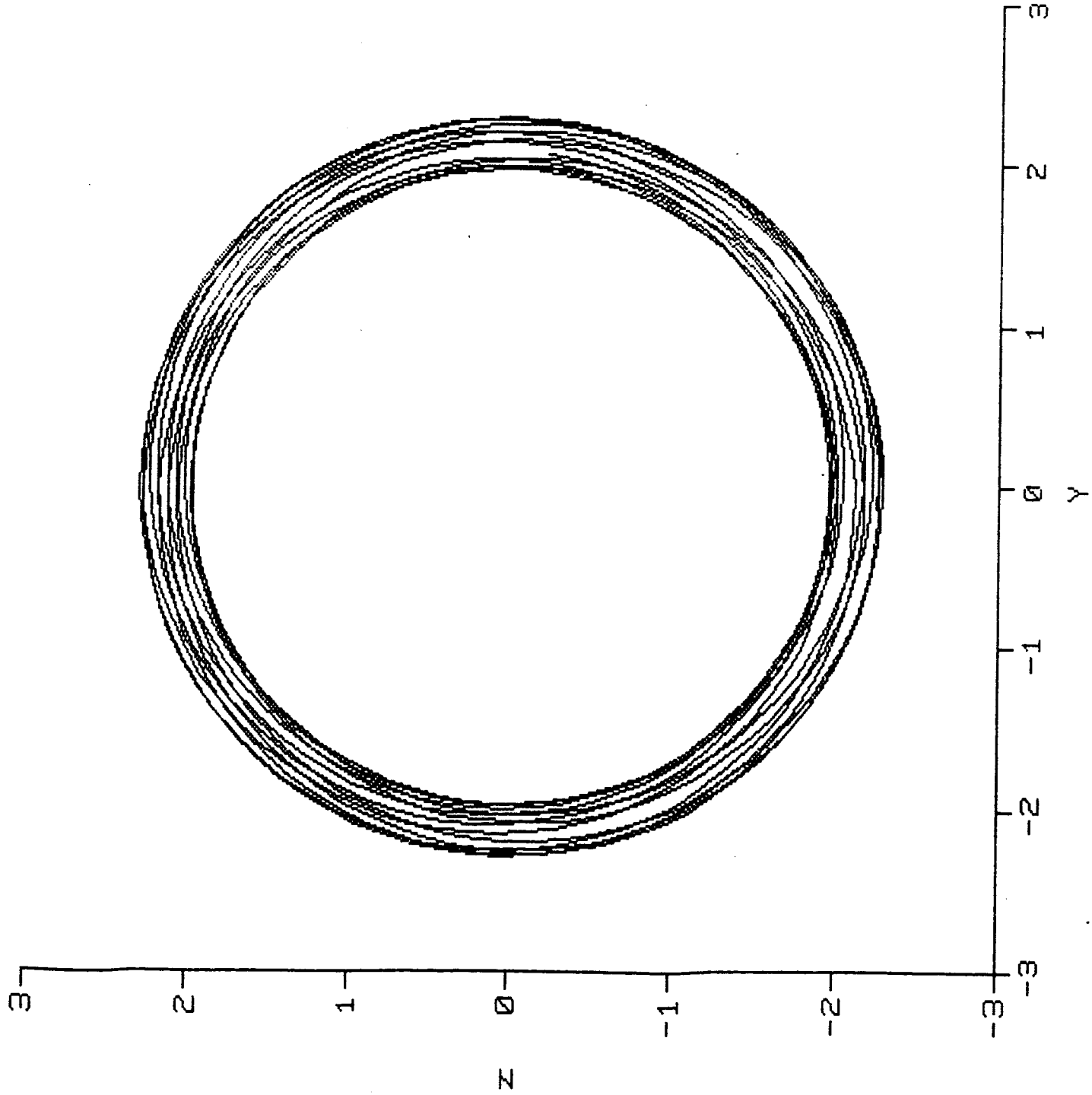

Figure 5

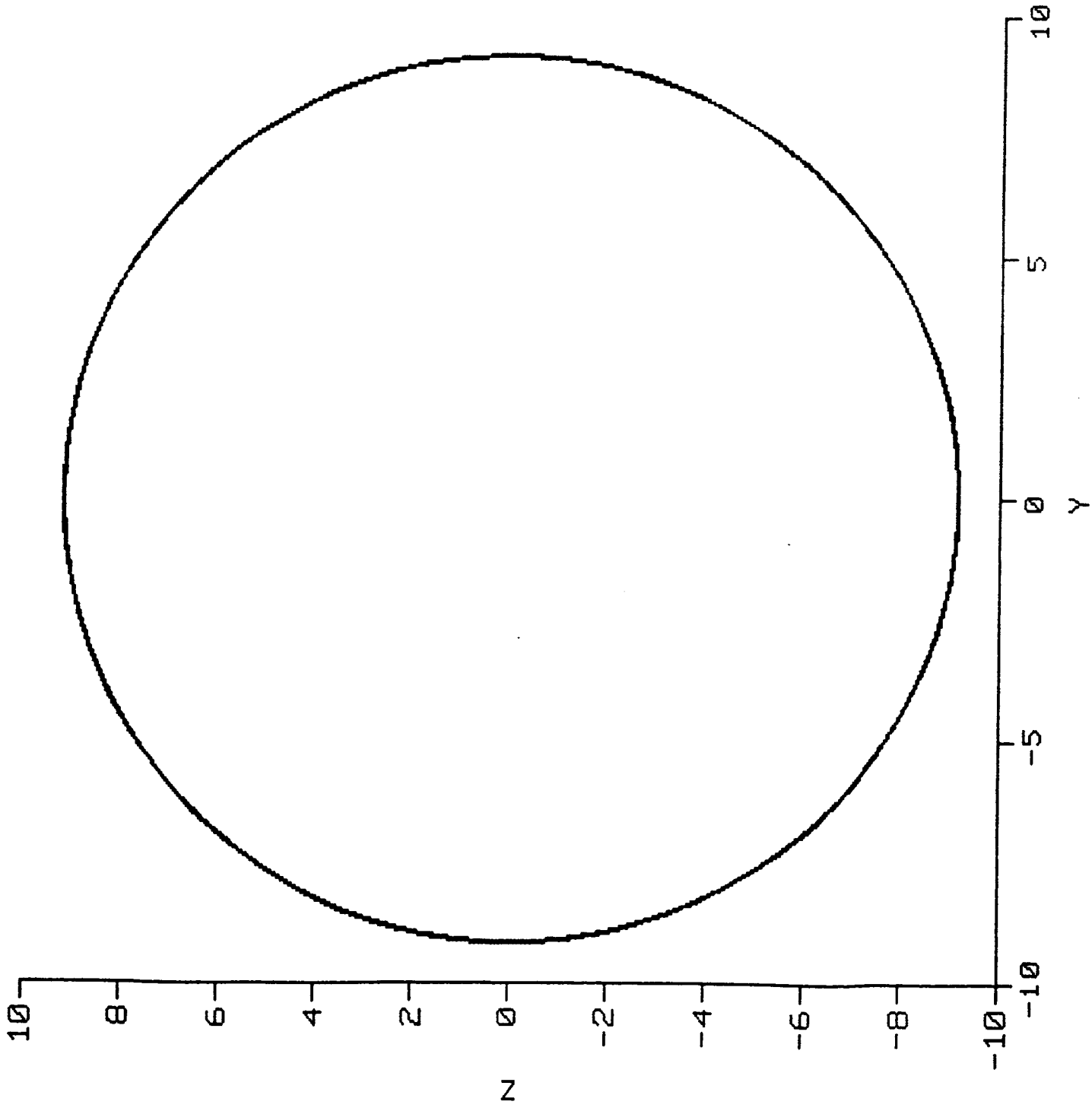

Figure 6

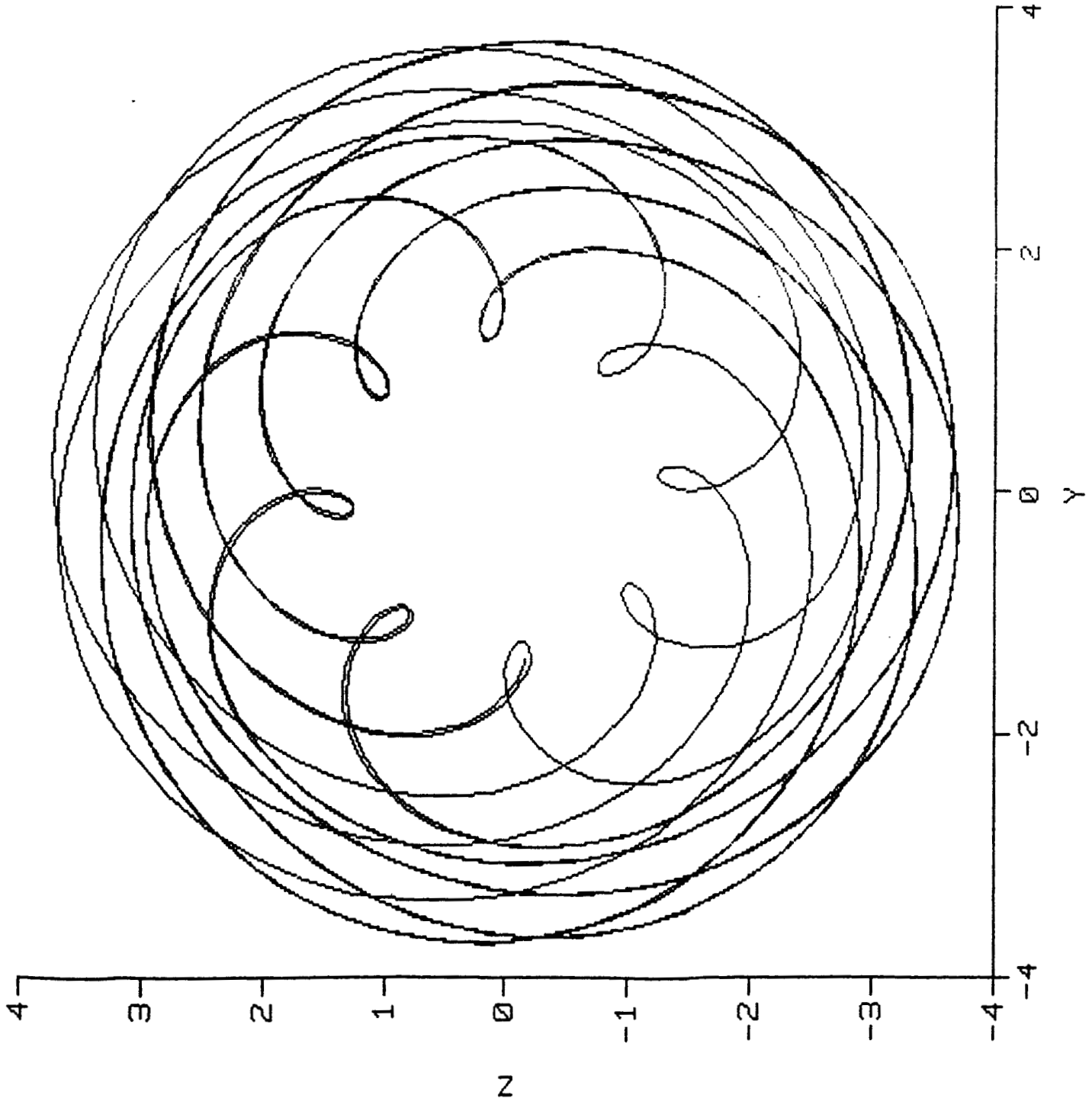

Figure 7

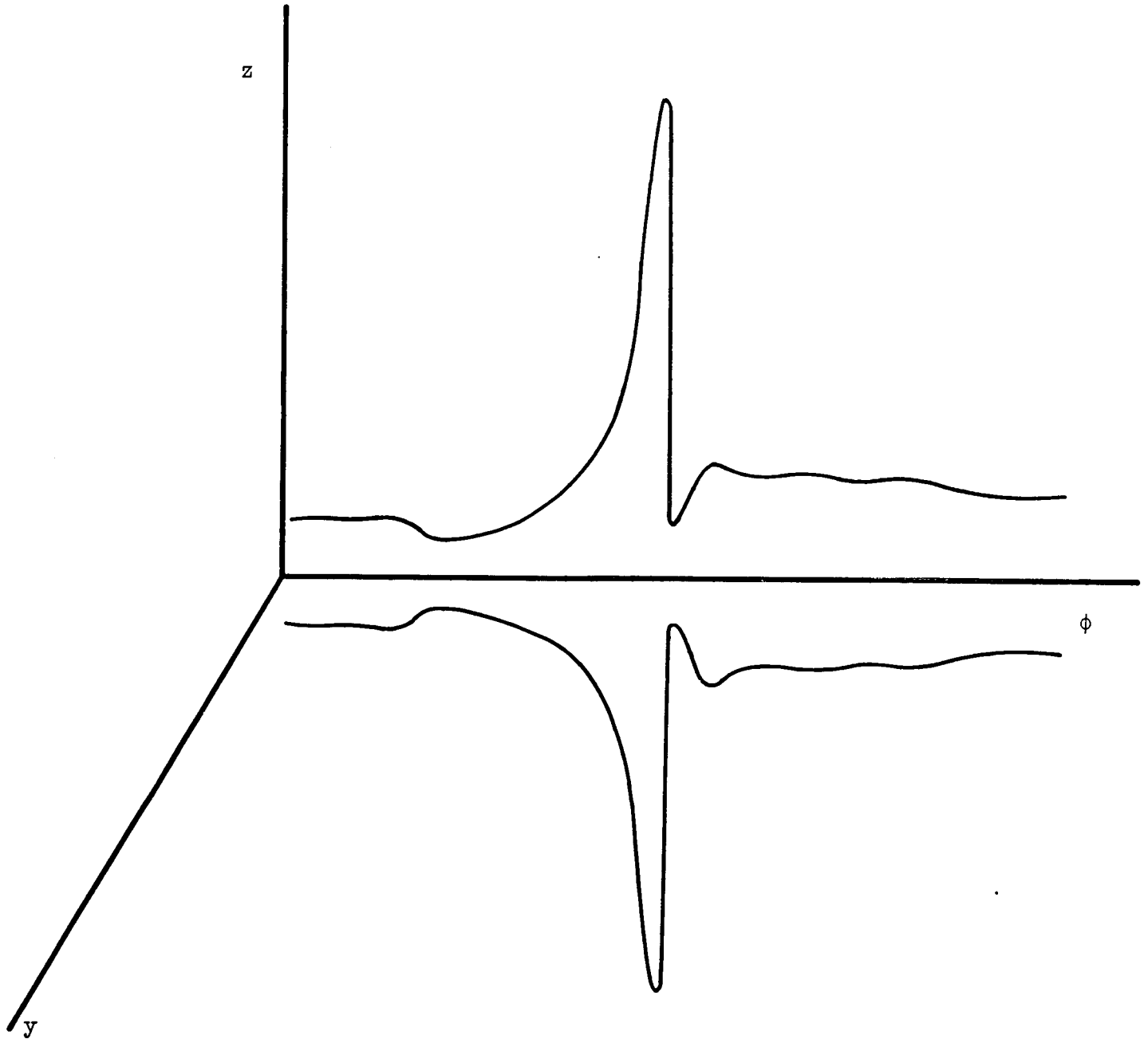

Figure 8

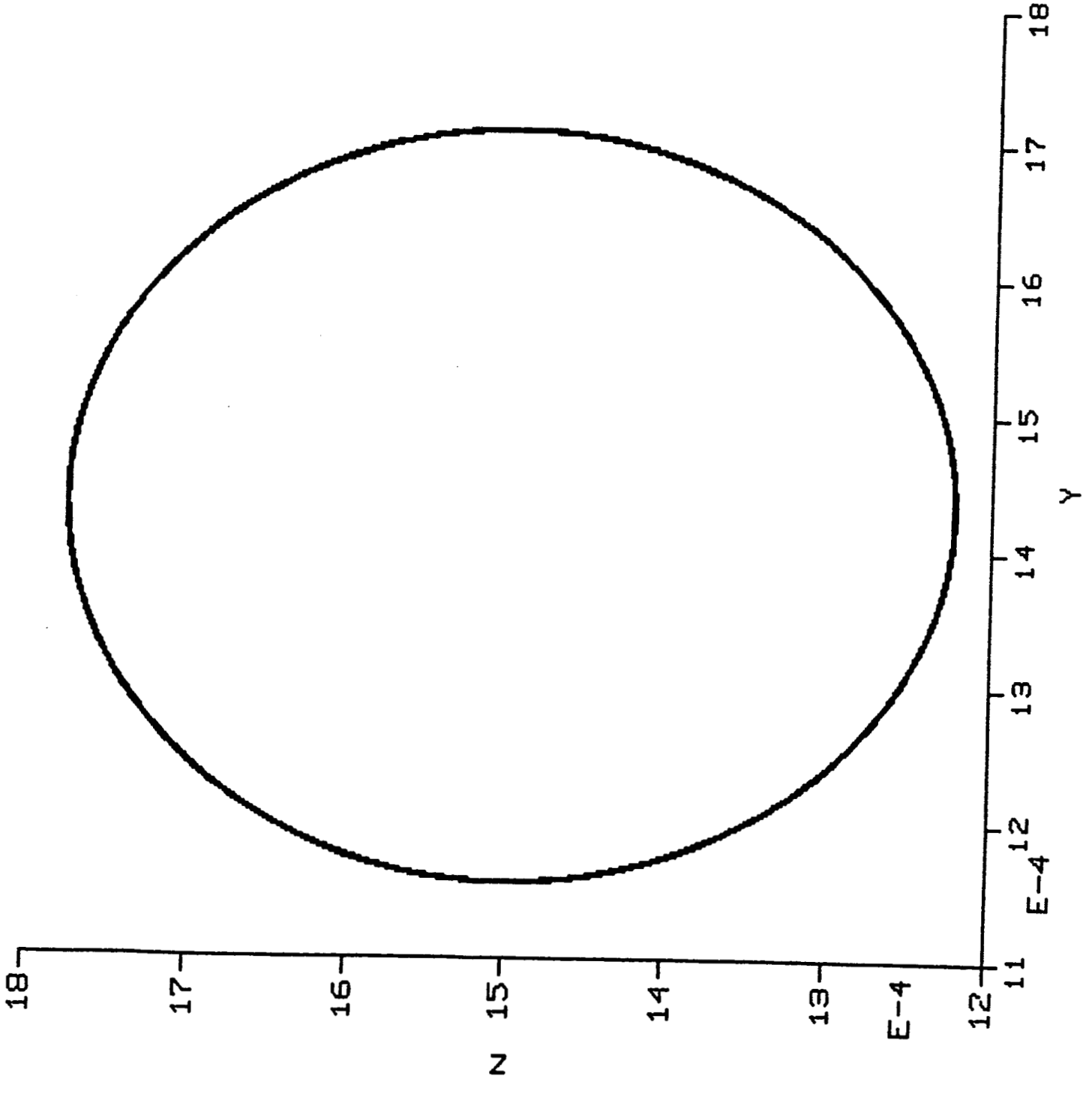

Figure 9

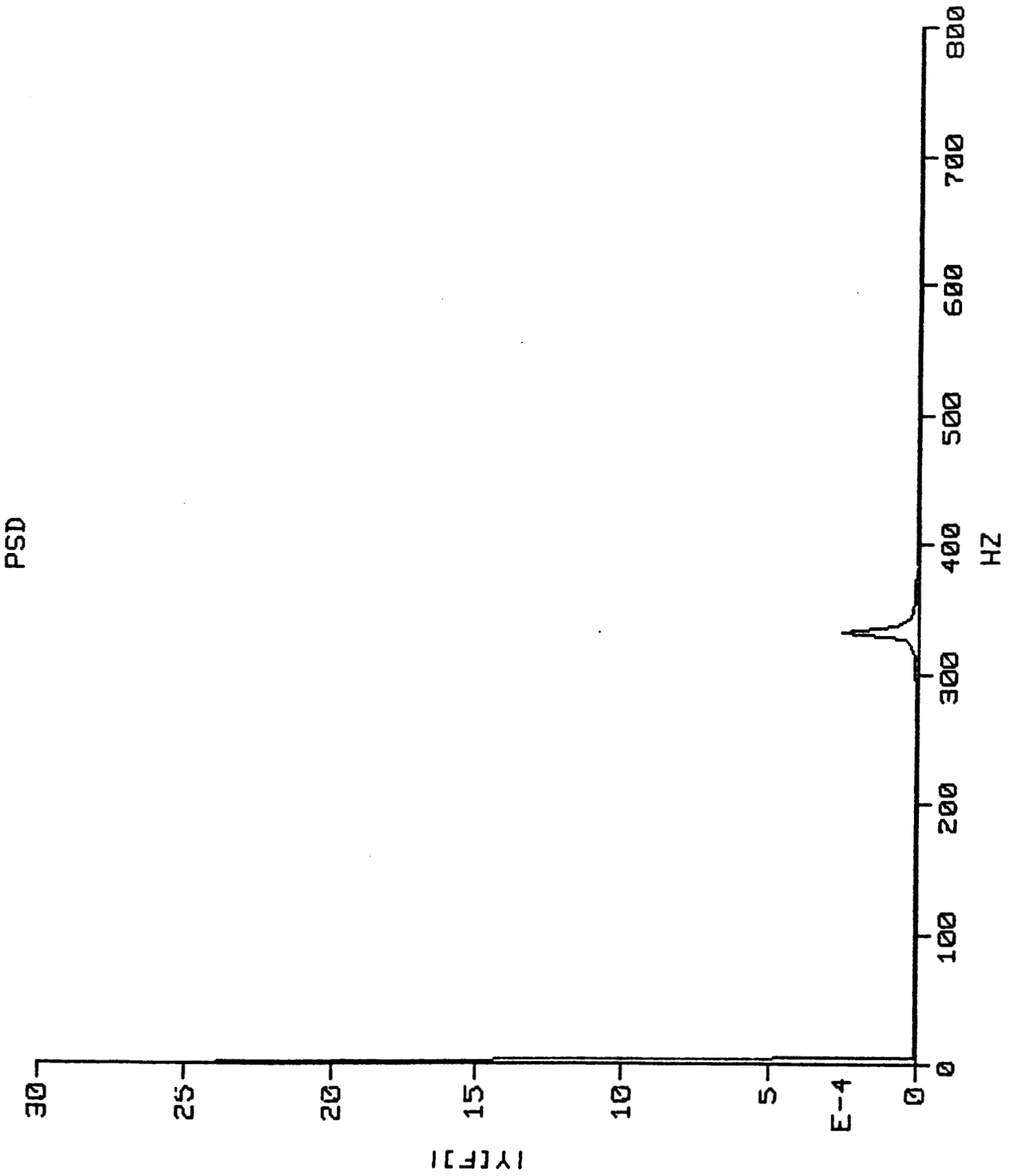

Figure 10

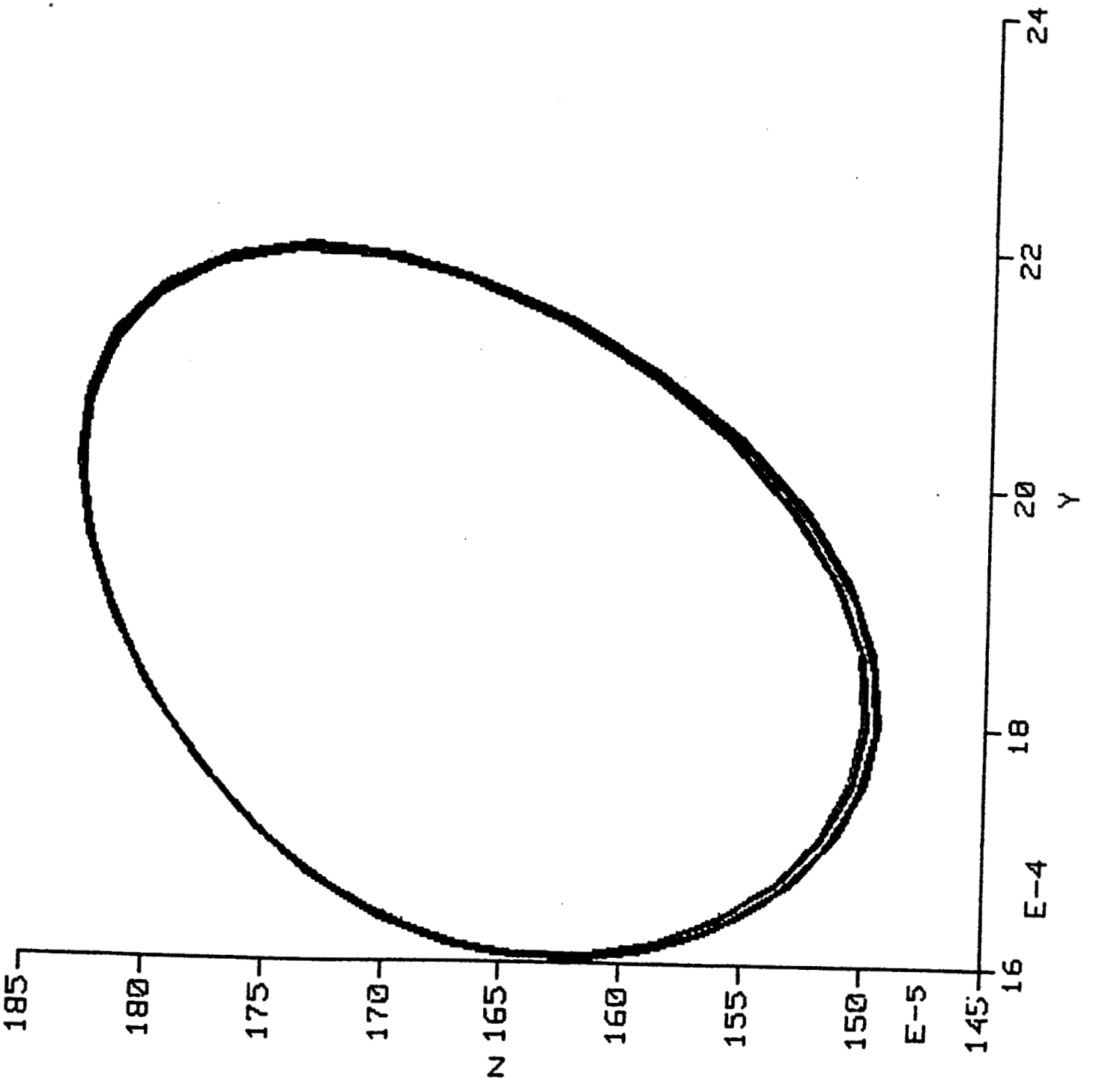

Figure 11

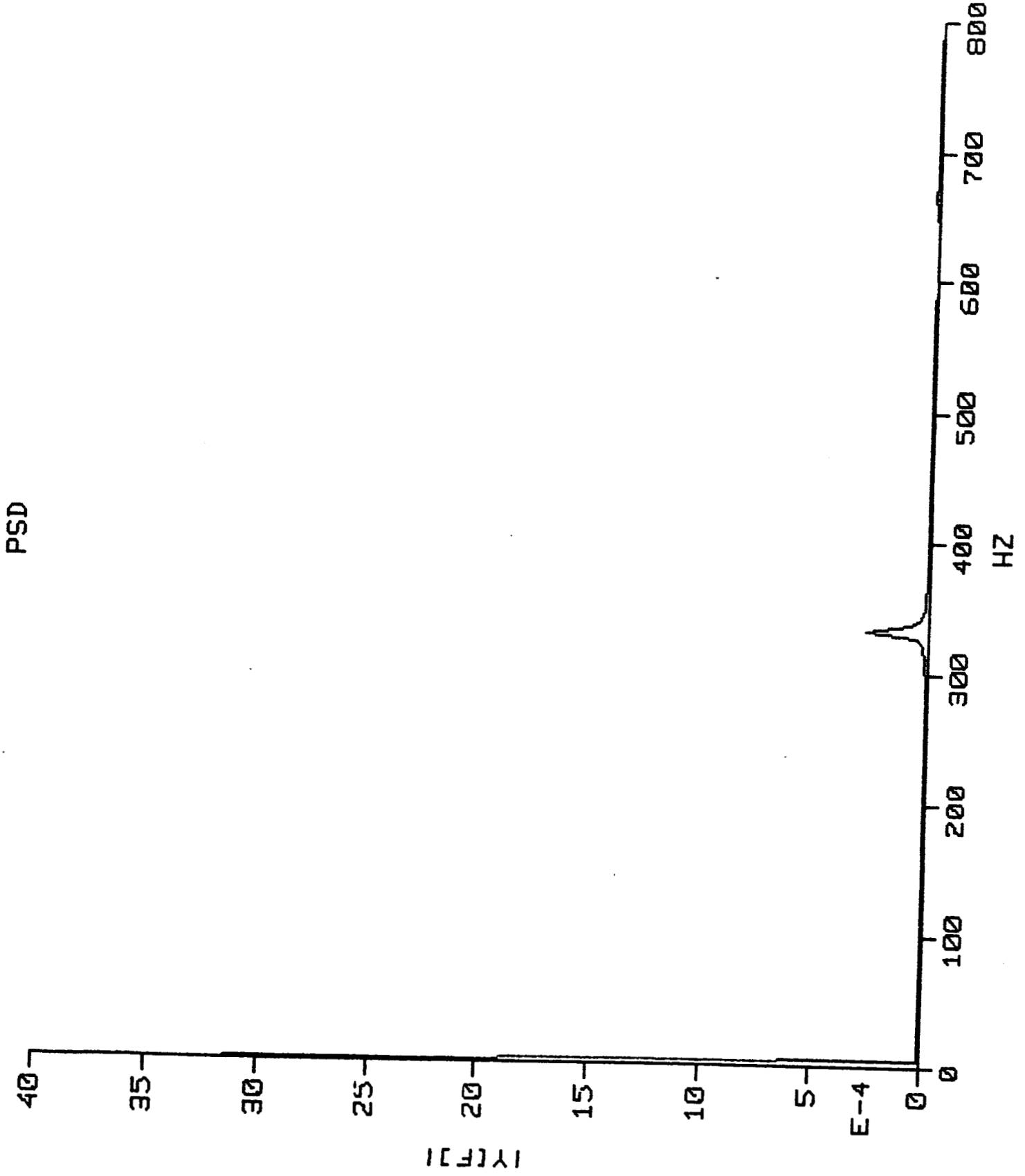

Figure 12

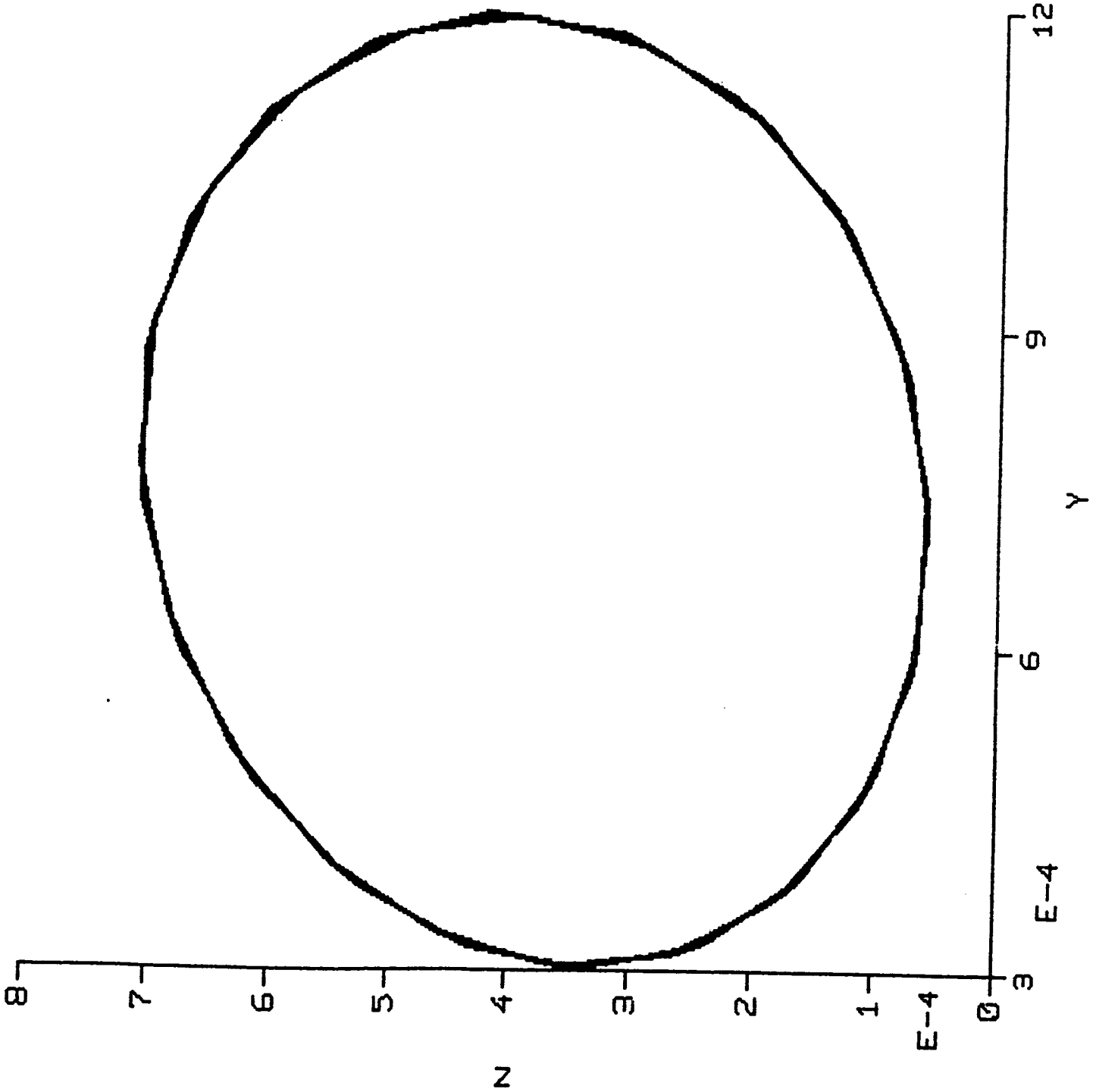

Figure 13

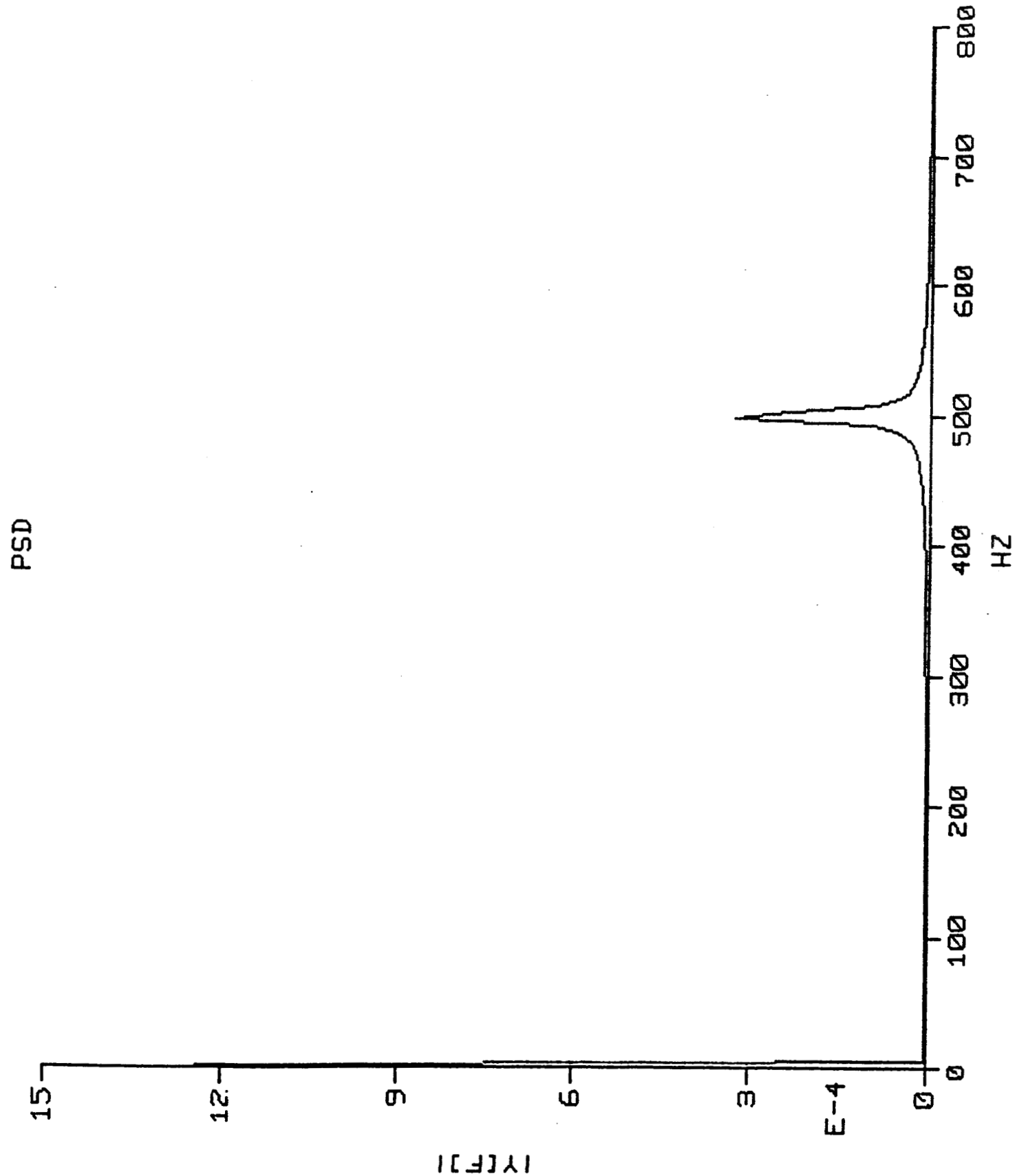

Figure 14

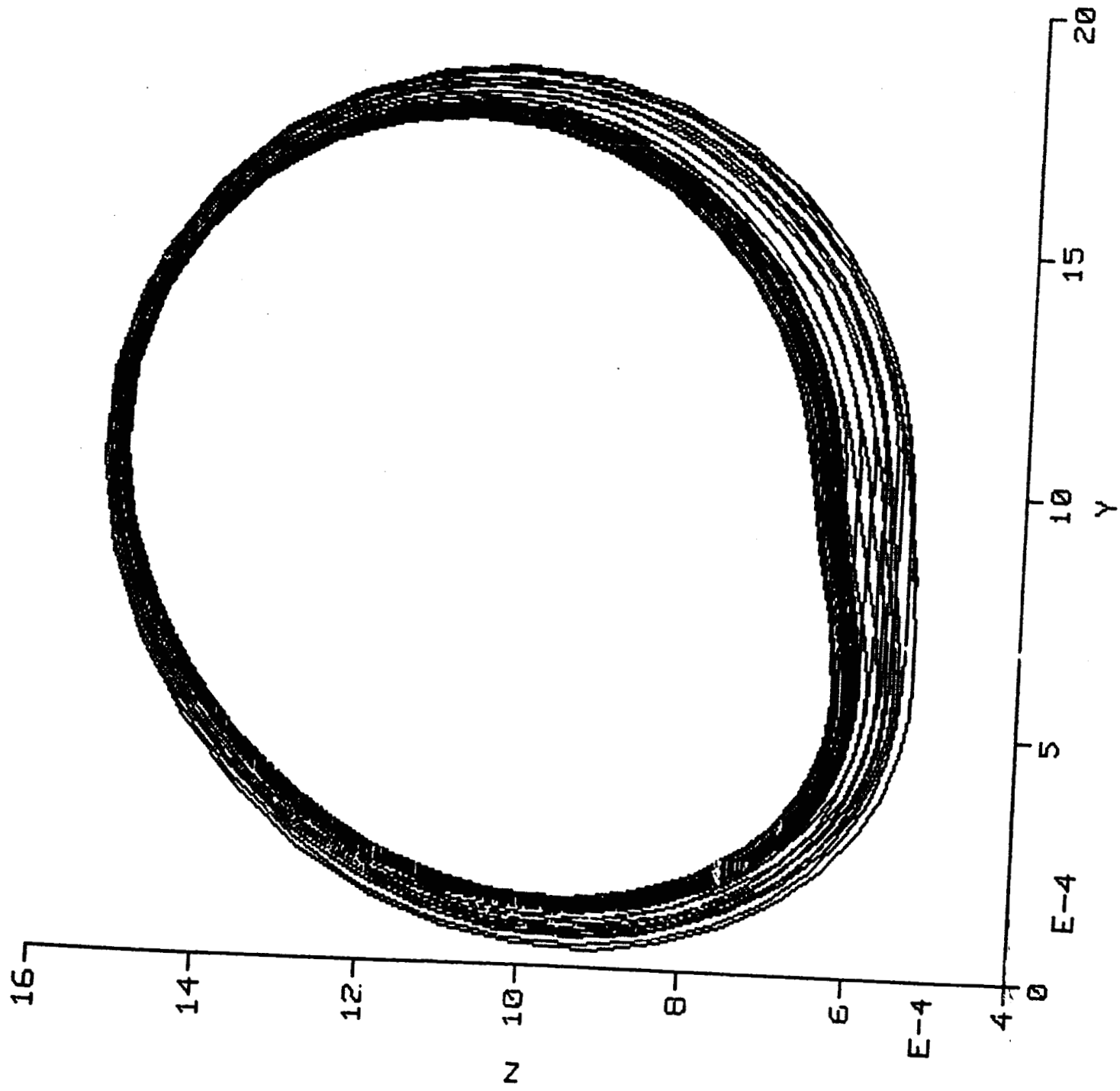

Figure 15

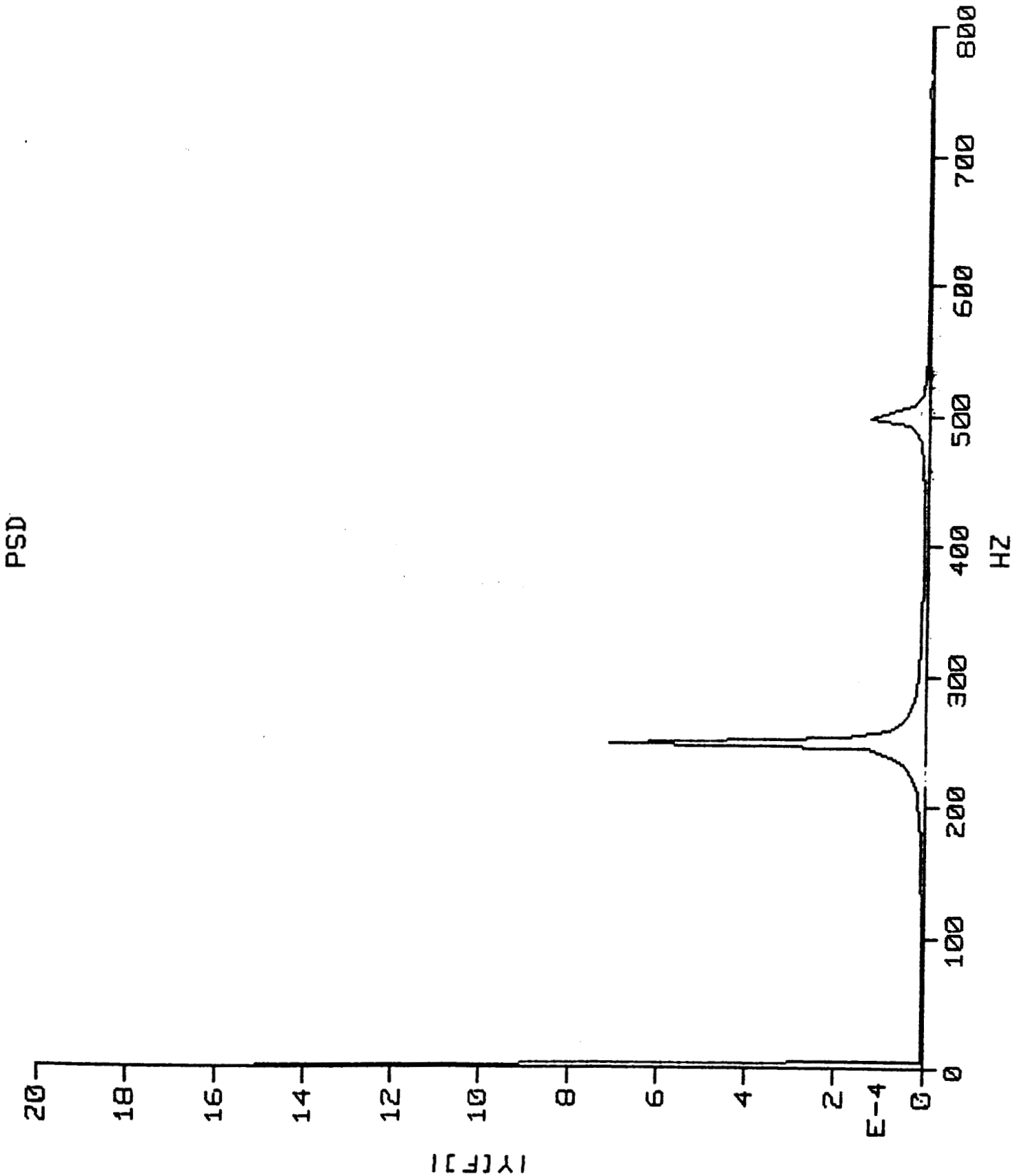

Figure 16

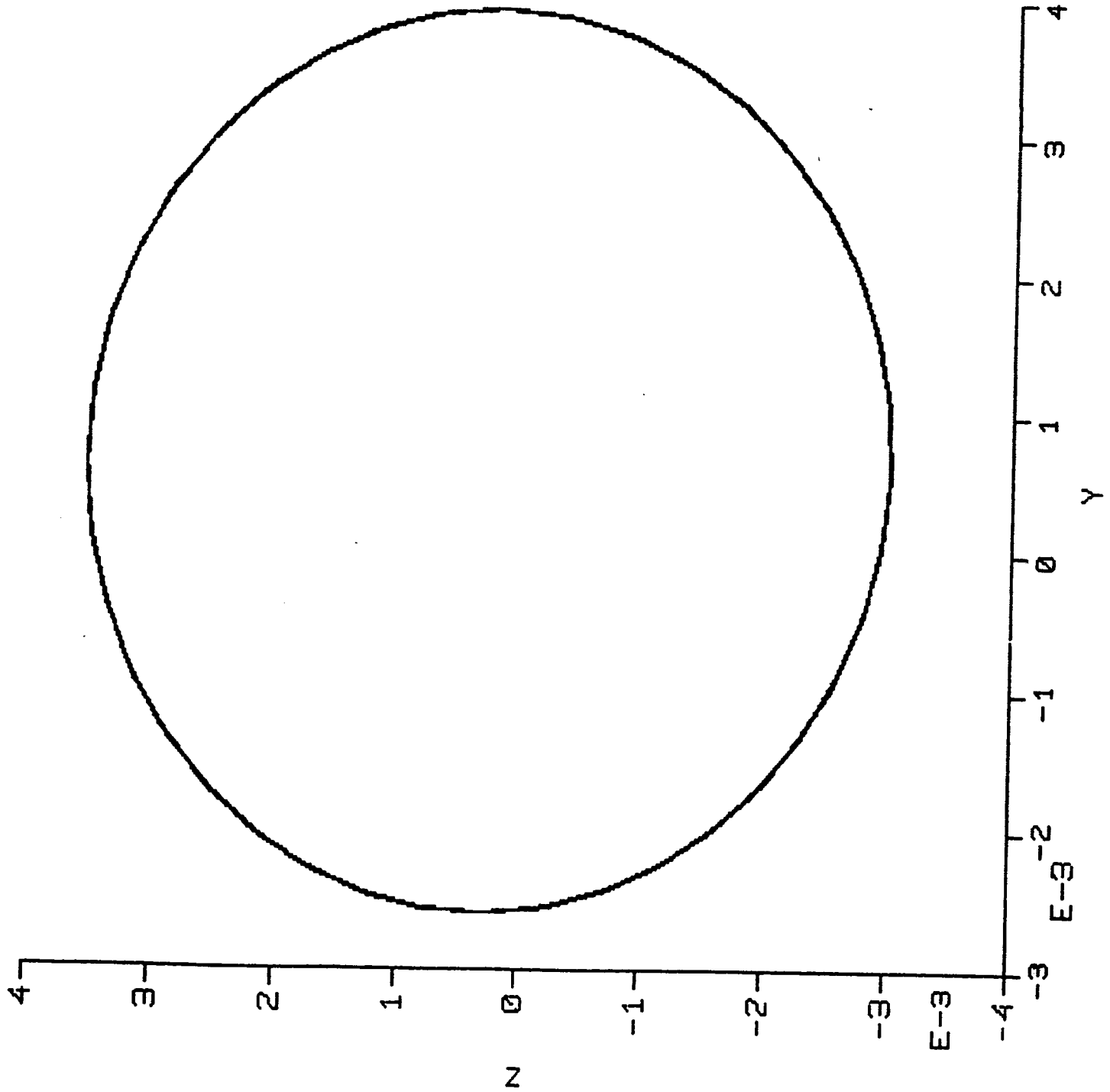

Figure 17

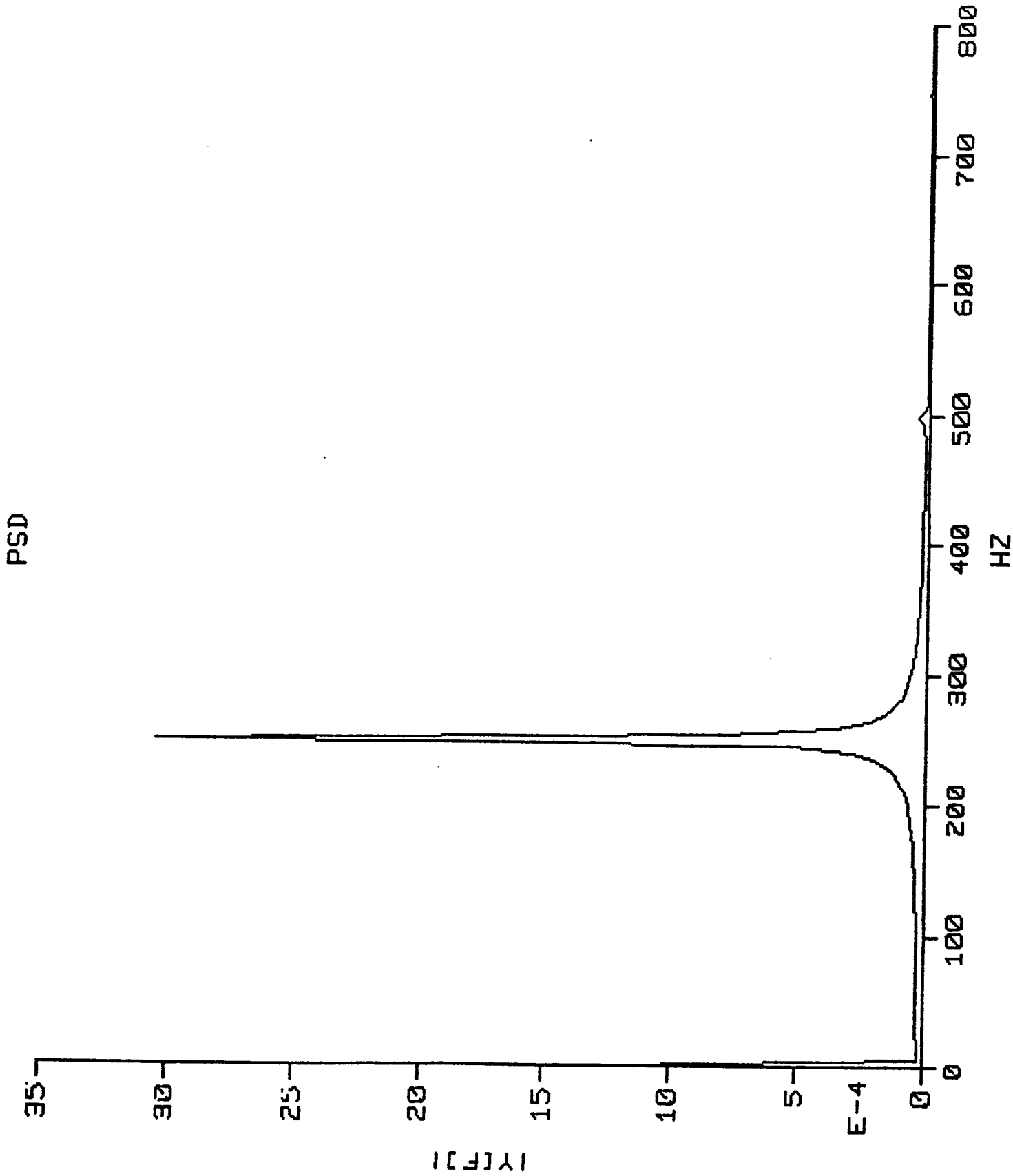

Figure 18

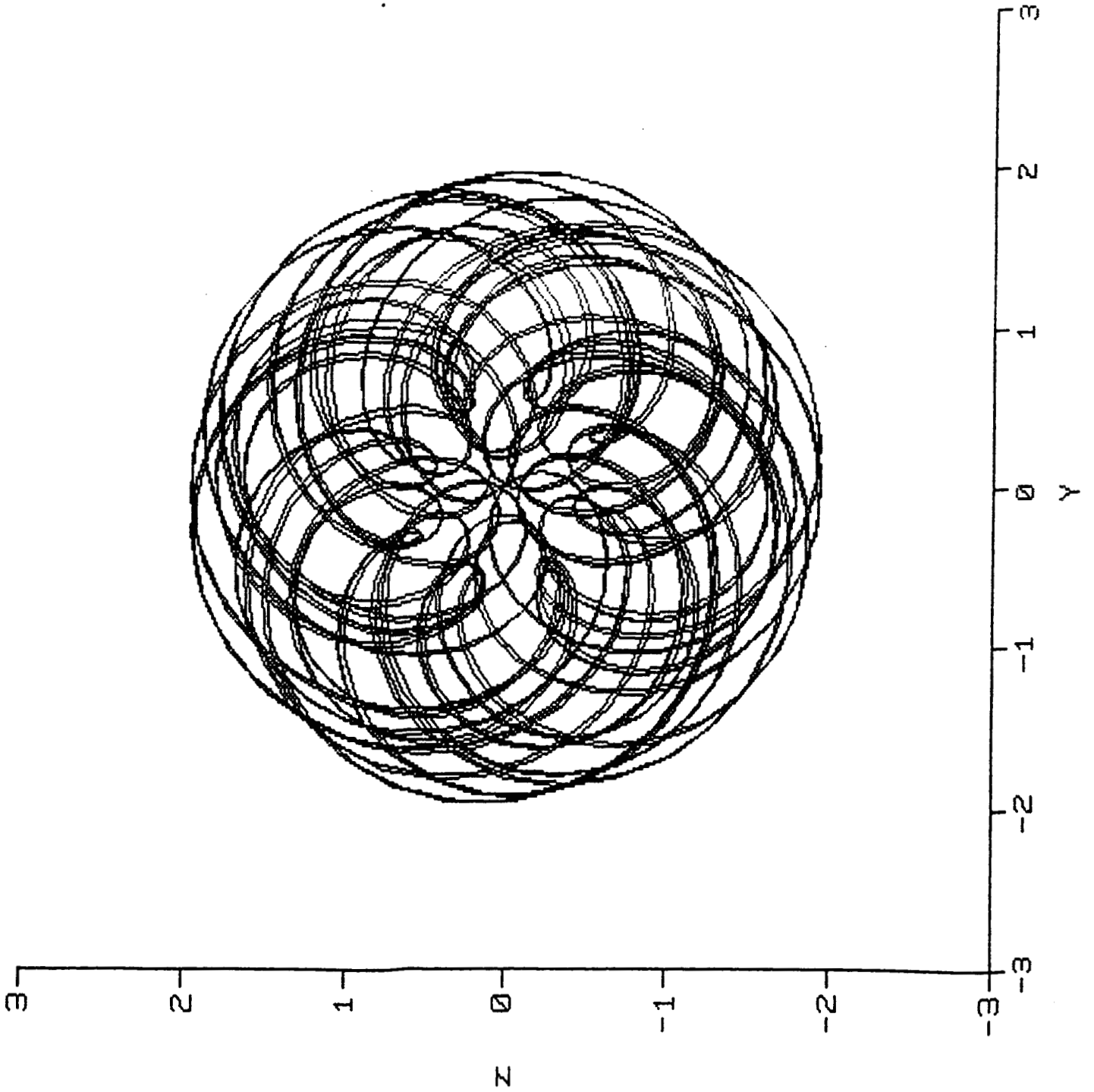

Figure 19

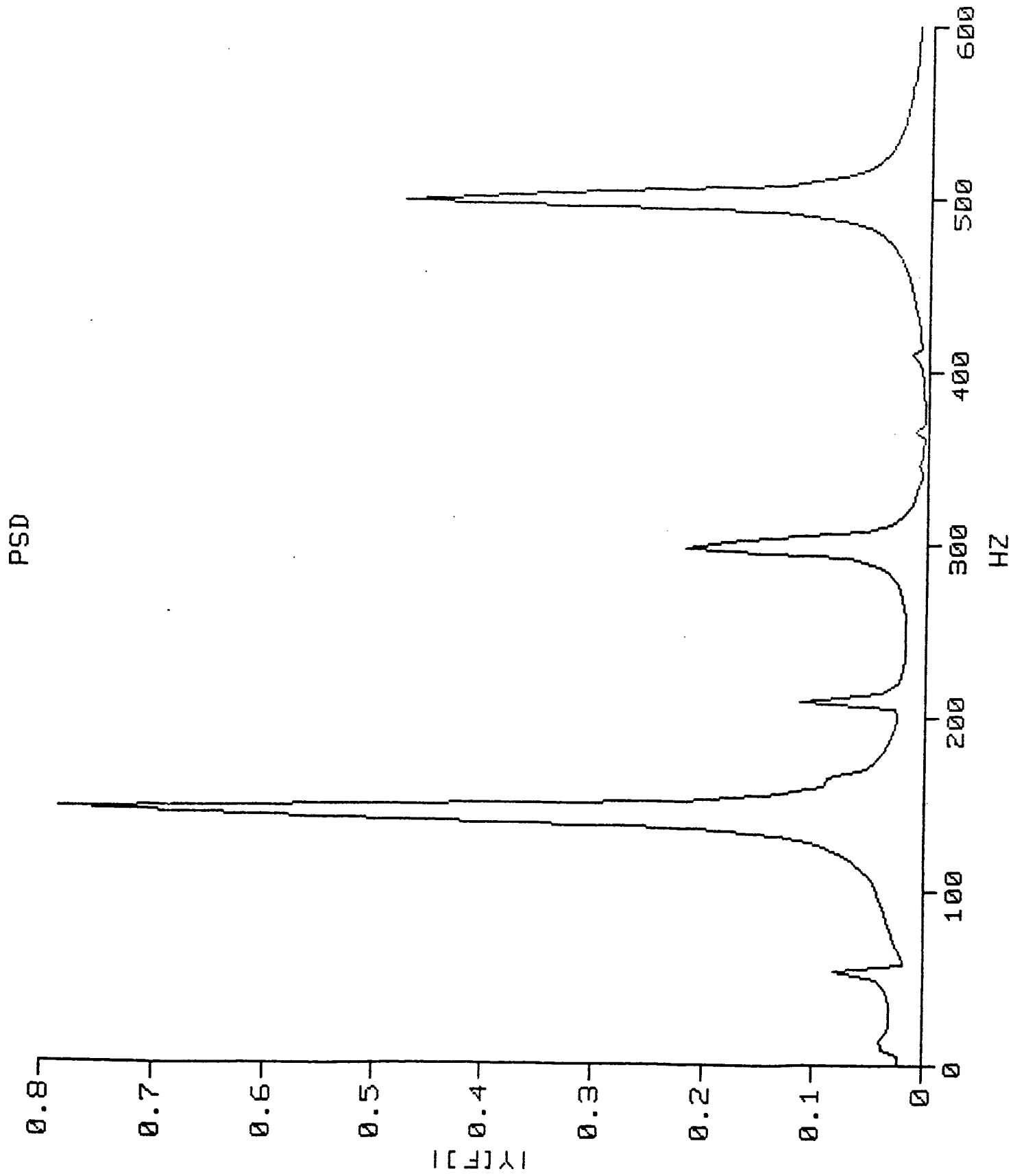

Figure 20

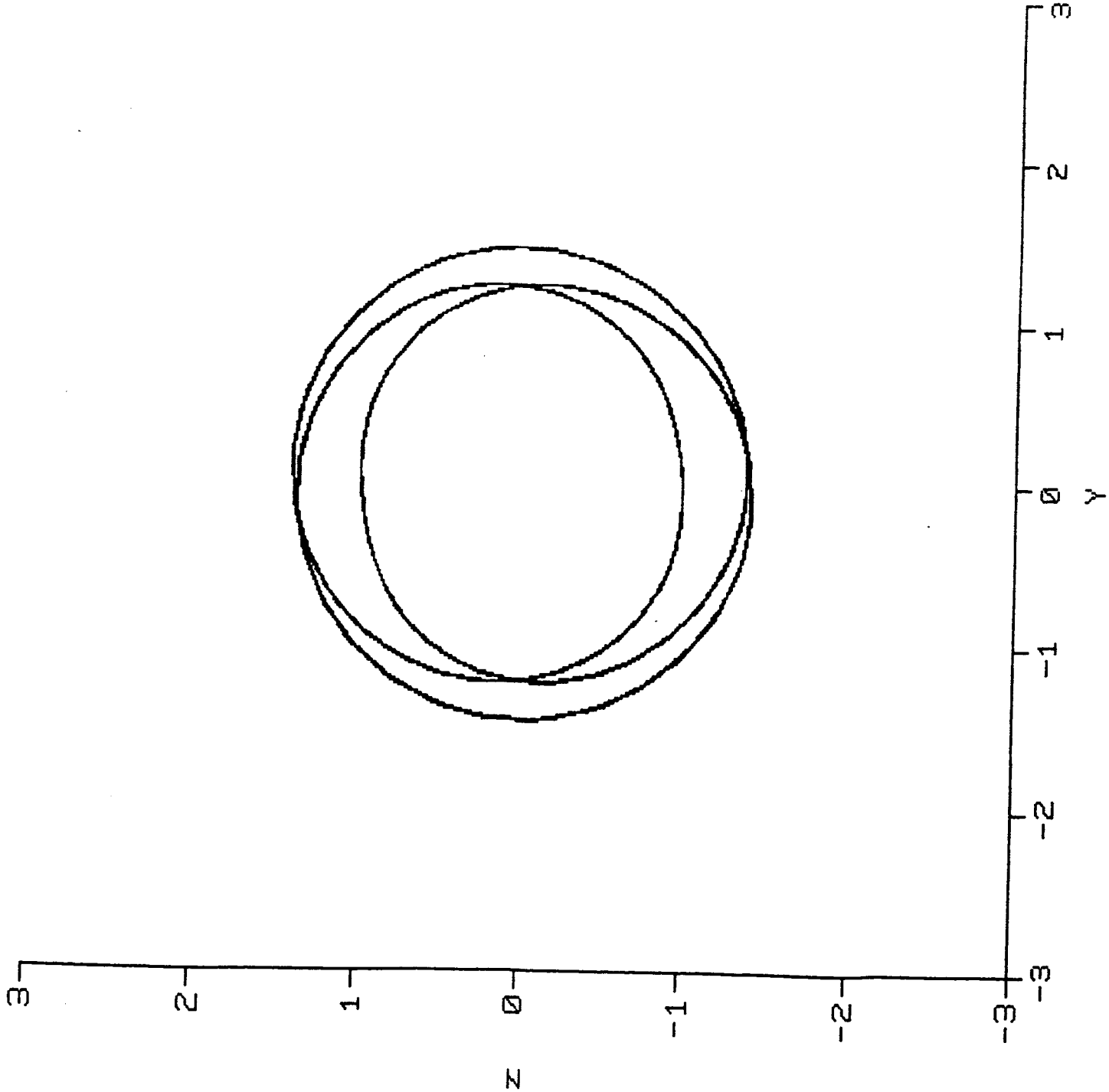

Figure 21

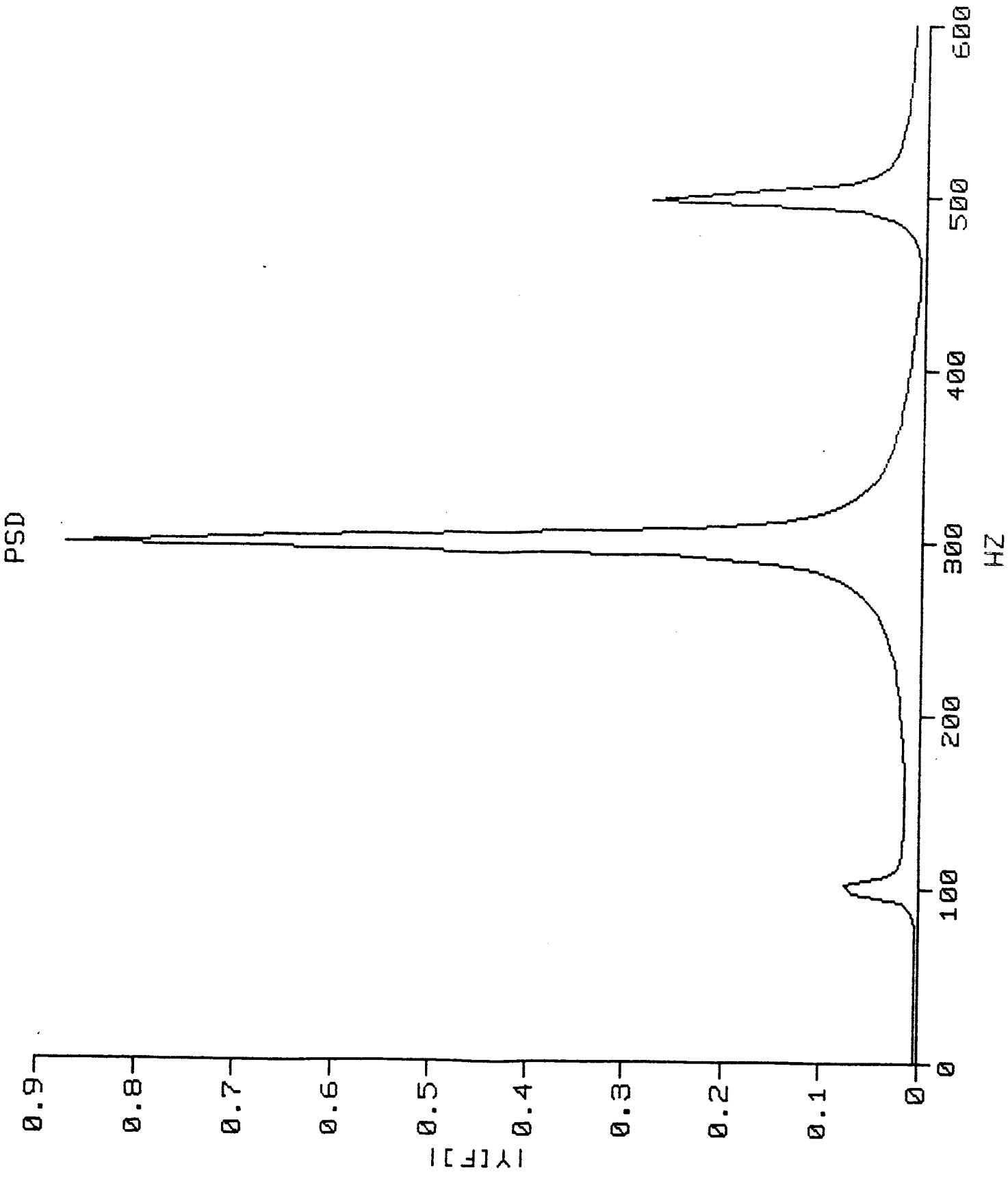

Figure 22

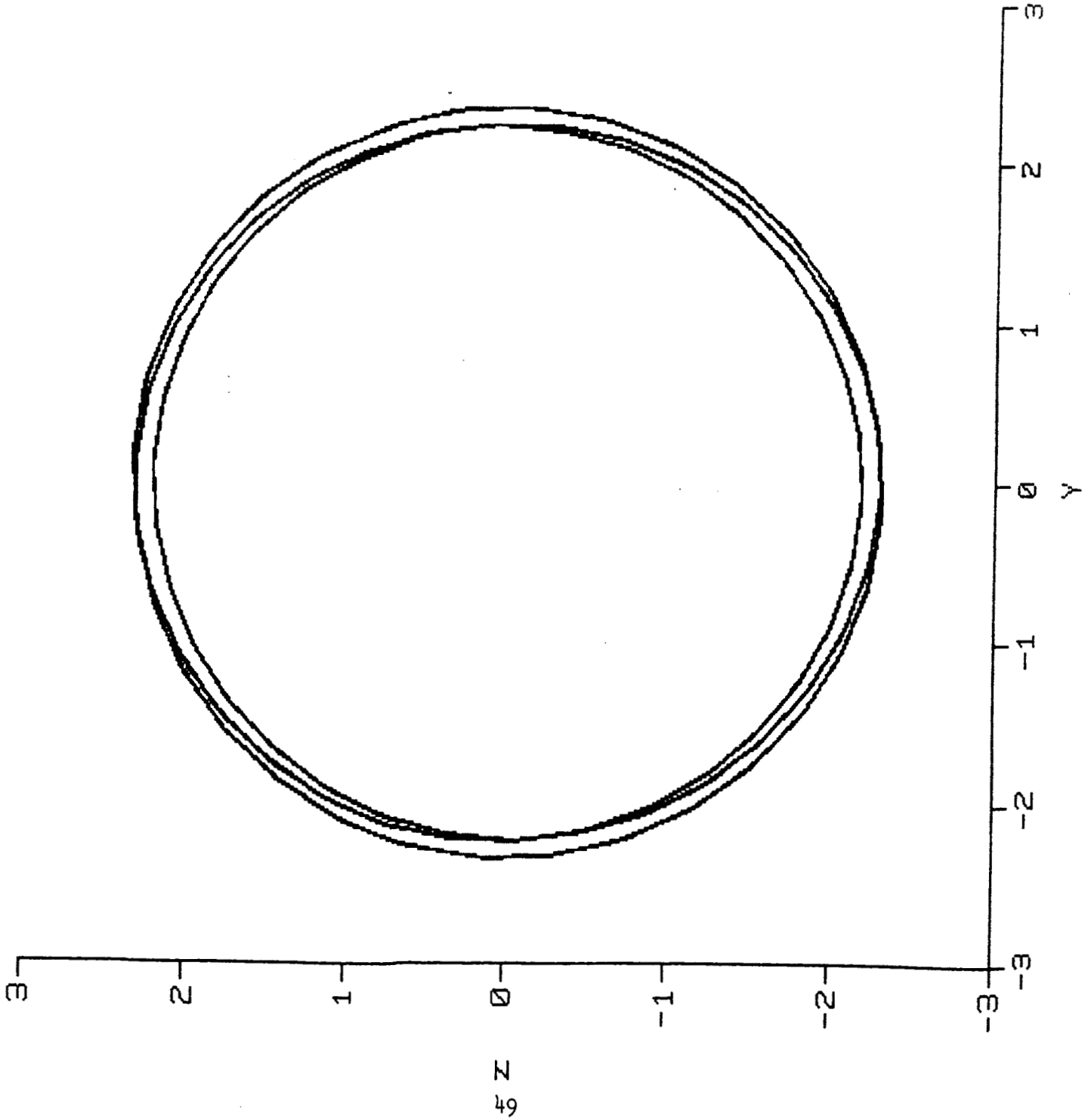

Figure 23

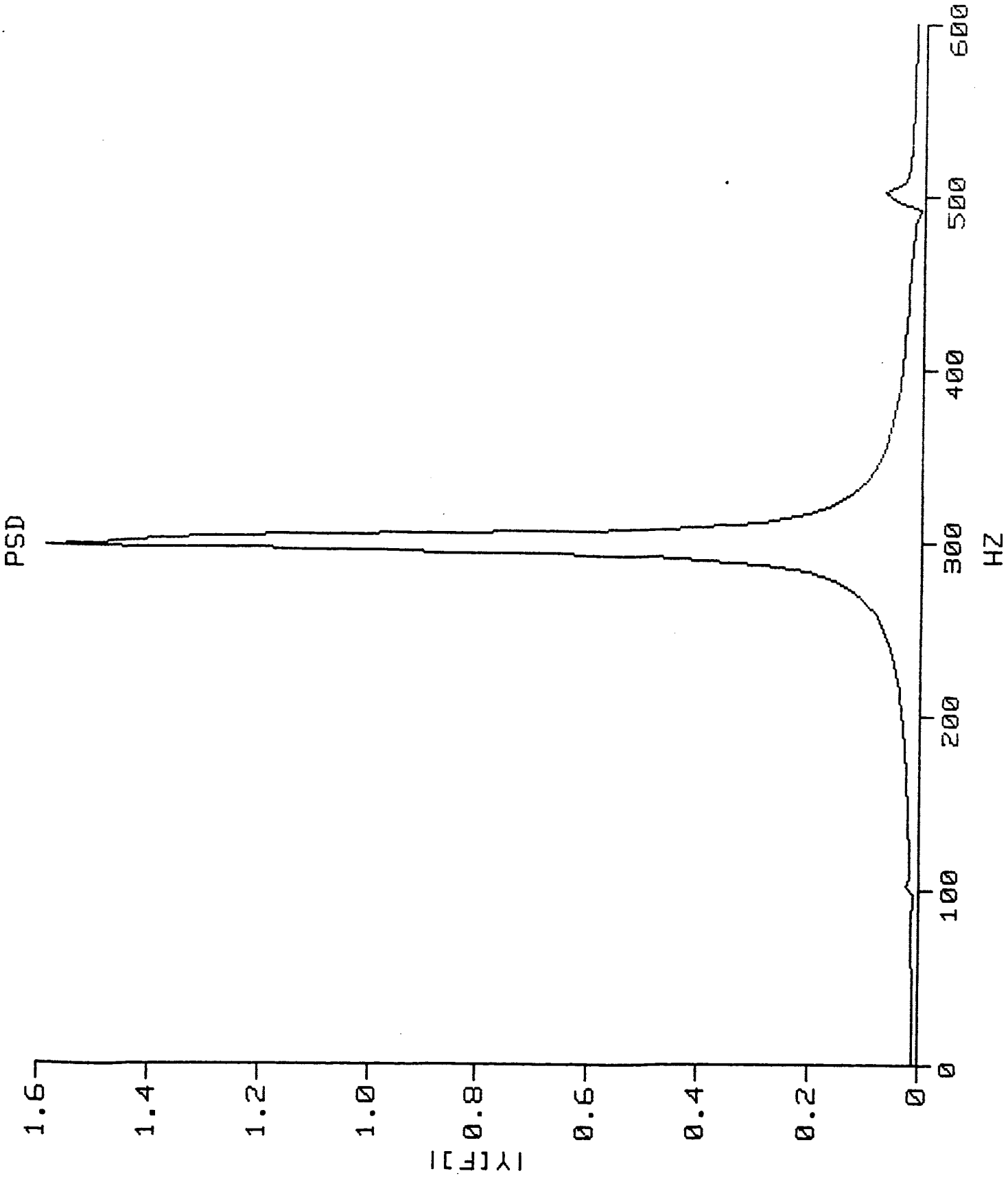

Figure 24

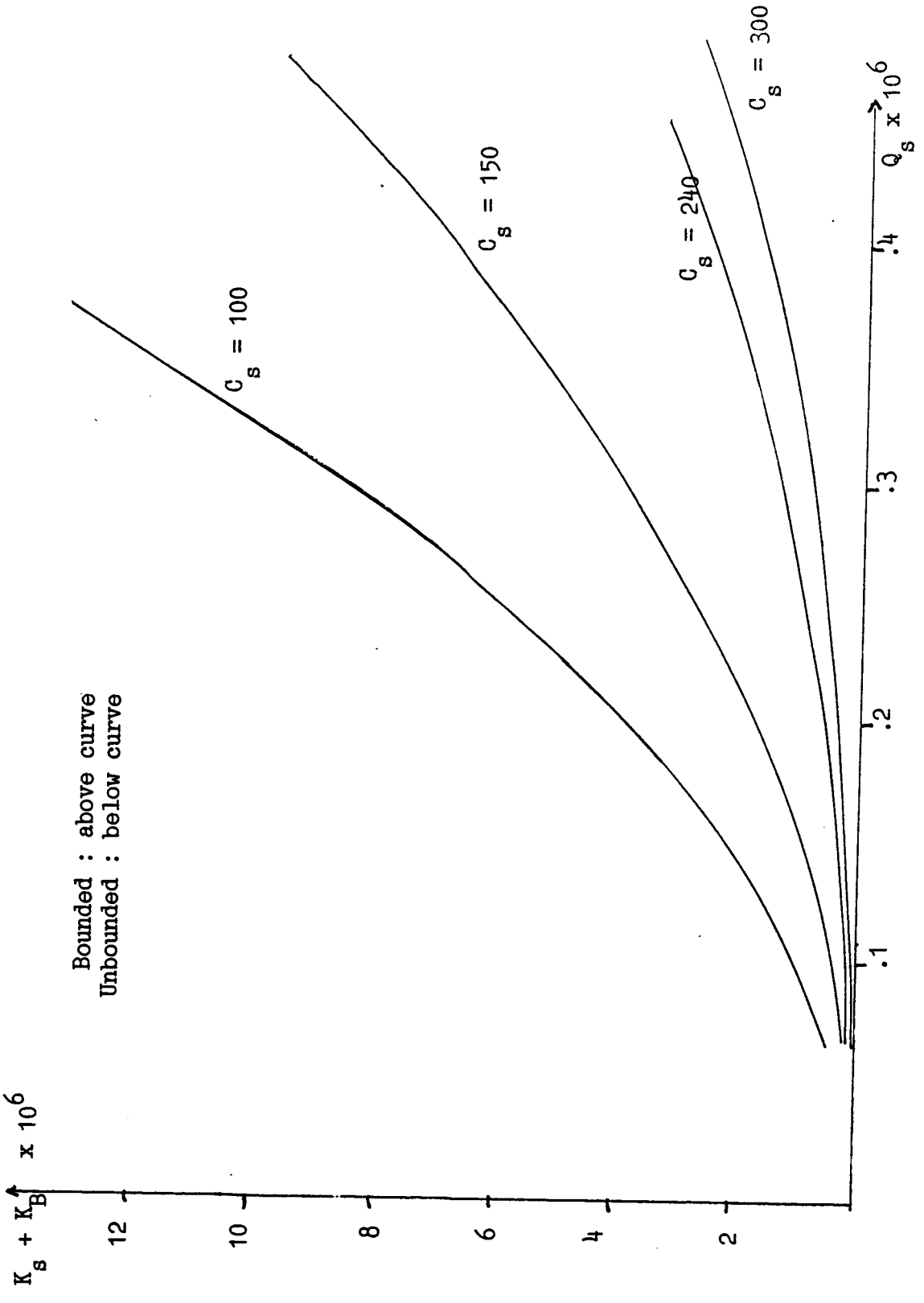
$K_s + K_B$ x 10^6
12
10
8
6
4
2
Bounded : above curve
Unbounded : below curve
C_s = 100
C_s = 150
C_s = 240
C_s = 300
.1
.2
.3
.4
Q_s x 10^6

Figure 25

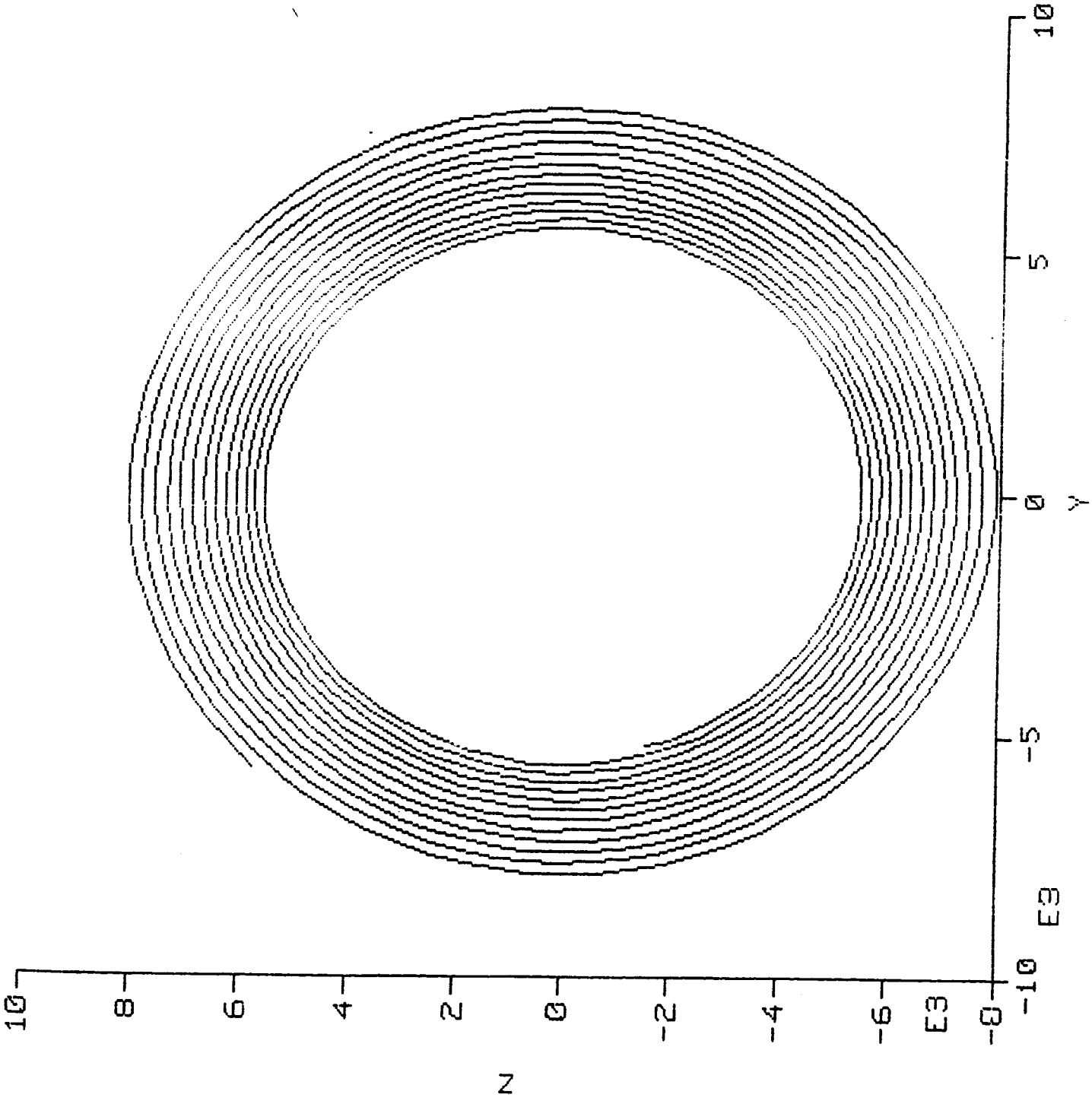

Figure 26

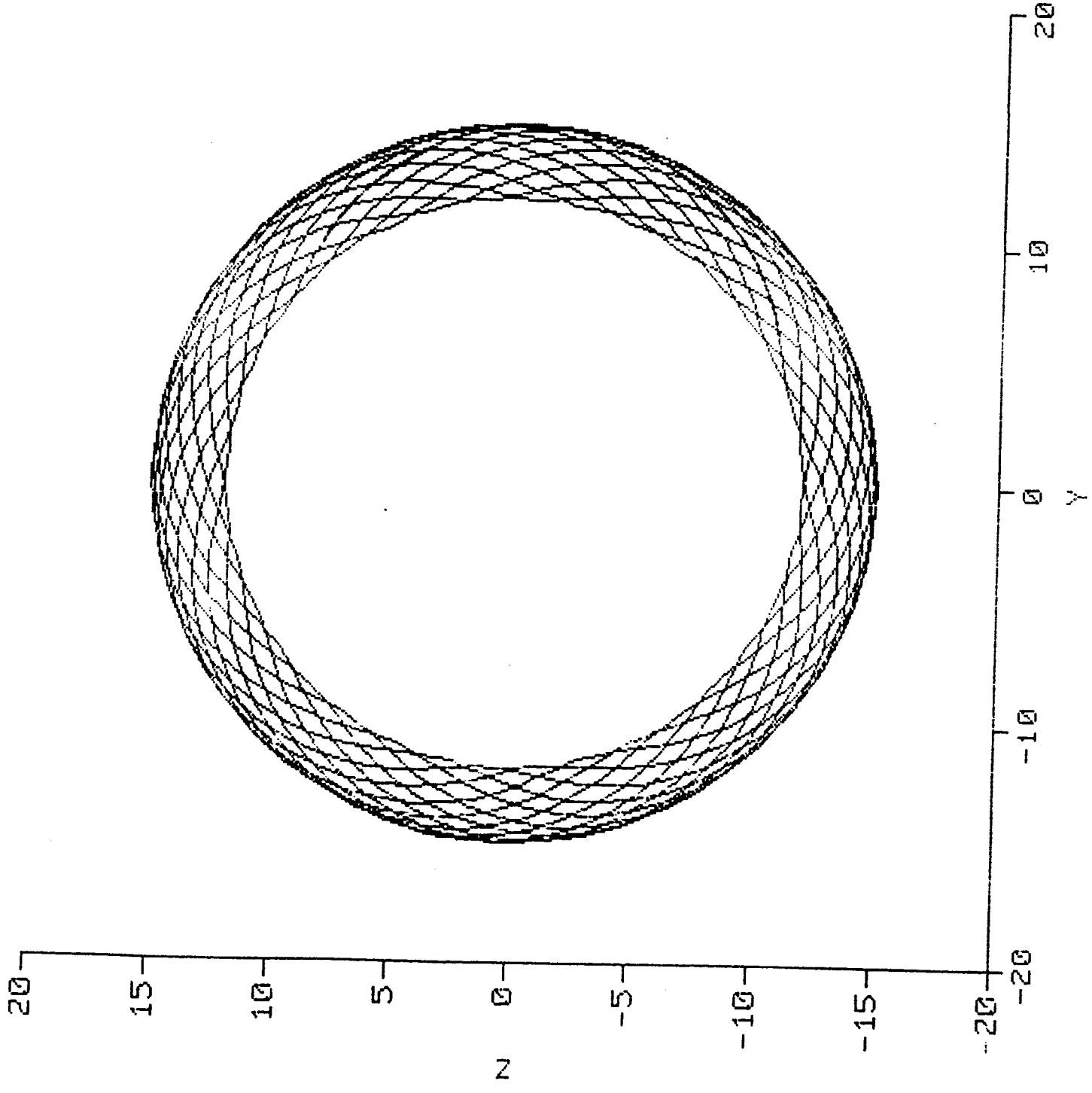

Figure 27

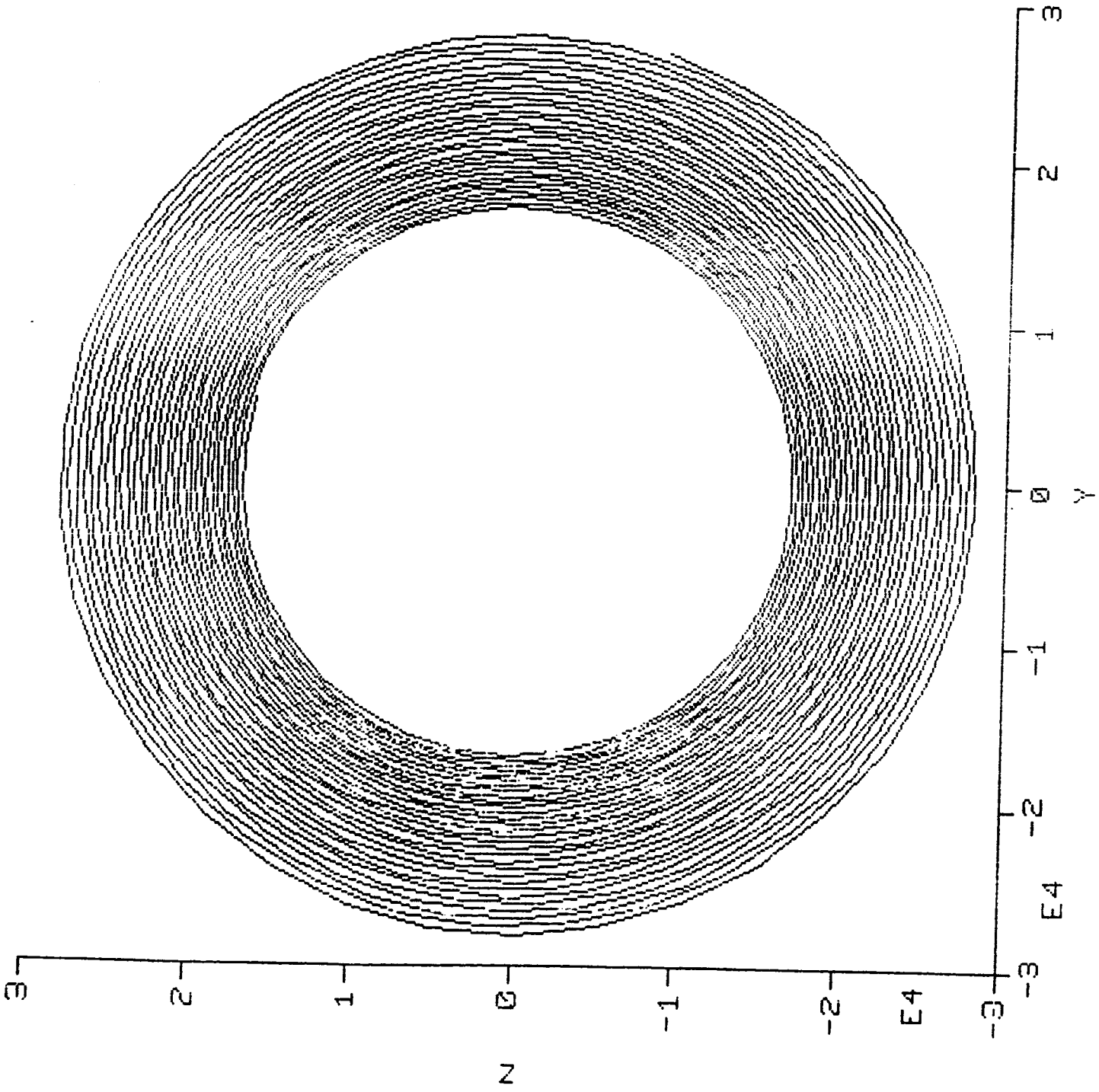

Figure 28

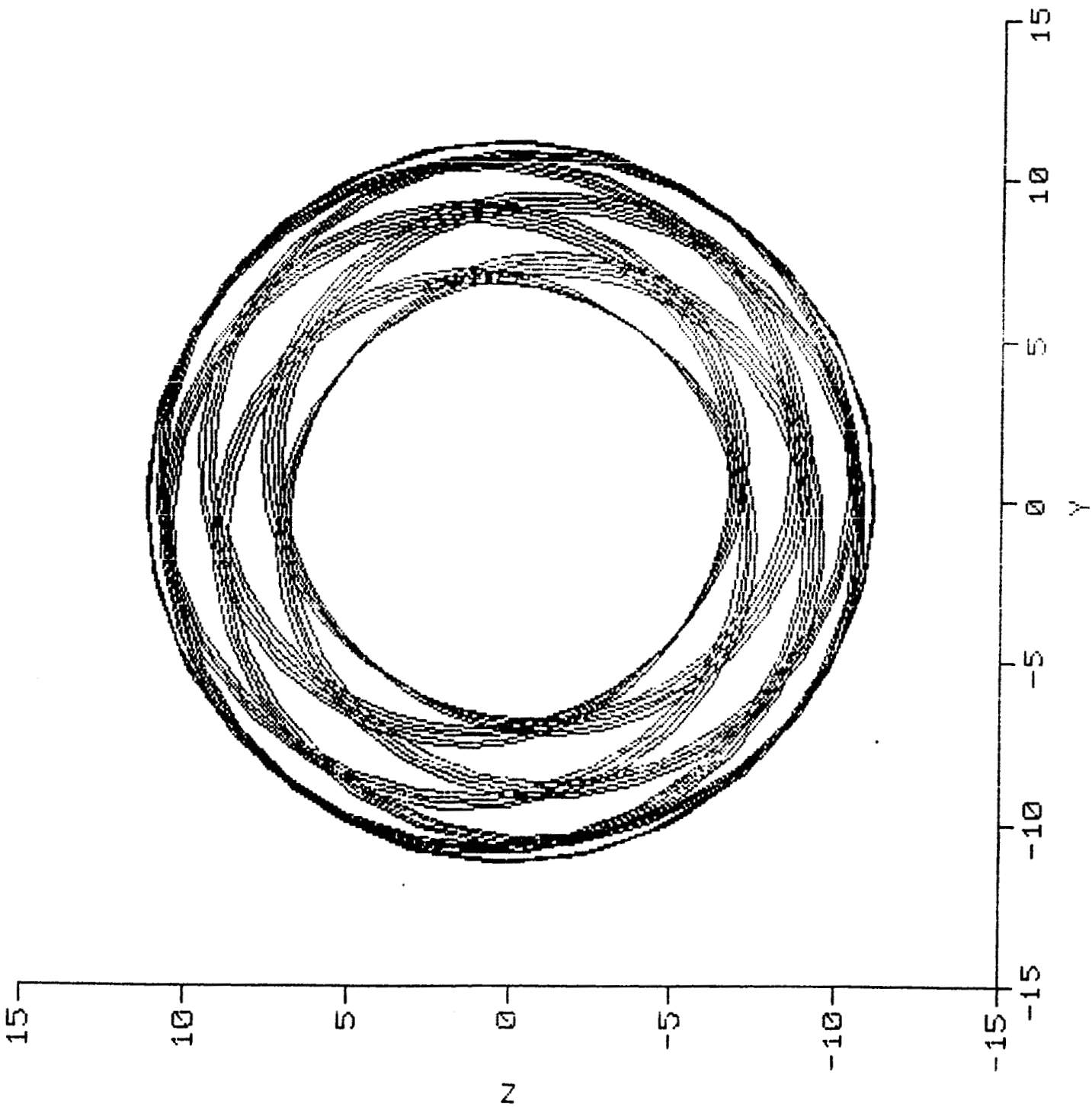

Table 1

Absolute coefficient values:
Ks = 0 Kb = 1305000 Cs = 240 Qs = 200000
eccentricity = .0000285 deadband = .00000285 omega = varied.

Nondimensionalizing parameters:
frequency = sqrt(Ks + Kb) = omega-naught = sqrt(1305000)
displacement = eccentricity = .0000285

Nondimensionalized coefficient values:
C = Cs/omega-naught = ND damping = 240/sqrt(1305000)
k = Kb/square(omega-naught) = ND stiffness = 1
B = Qs/square(omega-naught) = ND X-stiffness = 200000/1305000
phi = omega/omega-naught = ND forcing frequency = varied
delta = deadband/eccentricity = ND deadband = 0.1

phi		R	shape (A=annulus, C=circle)	
0.0		0.21	C	annulus for phi
0.1		0.20-0.23	A	between 0.0 and 0.11
0.2		0.14	C	
0.3		0.21	C	
0.4		0.31	C	
0.5		0.47	C	circle for phi
0.6		0.72	C	greater than 0.12
0.7		1.16	C	
0.8		2.05	C	
0.9		4.70	C	
1.0	<PEAK>	17.48	C	
1.1		4.97	C	
1.2		2.97	C	
1.3		2.27	C	
1.4		1.92	C	
1.5		1.71	C	
1.6		1.57	C	
1.7		1.47	C	
1.8		1.39	C	
1.9		1.34	C	
2.0		1.29	C	

Table 2

Absolute coefficient values:
Ks = 0 Kb = 1305000 Cs = 240 Qs = 200000
eccentricity = .0000285 = deadband omega = varied

Nondimensionalizing parameter:
frequency = sqrt(Ks + Kb) = omega-naught = sqrt(1305000)
displacement = eccentricity = .0000285

Nondimensionalized coefficient values:
C = Cs/omega-naught = ND damping = 240/sqrt(1305000)
k = Kb/square(omega-naught) = ND stiffness = 1
B = Qs/square(omega-naught) = ND X-stiffness = 200000/1305000
phi = omega/omega-naught = ND forcing frequency = varied
delta = deadband/eccentricity = ND deadband = 1

phi		R	shape (A=annulus, C=circle)	
0.0		2.14	C	
0.1		2.12-2.15	A	annulus for phi
0.2		2.07-2.20	A	between 0.00 and 0.31
0.3		1.97-2.30	A	
0.4		1.35	C	
0.5		1.65	C	
0.6		2.12	C	circle for phi
0.7		2.92	C	between 0.32 and 0.99
0.8		4.55	C	
0.9		9.17	C	
0.97	(PEAK)	18.52	C	
1.0		0.87-2.04	A	
1.1		0.77-4.56	A	
1.2		1.01-3.94	A	annulus for phi
1.3		1.12-3.93	A	greater than 1.0
1.4		1.14-3.97	A	
1.5		1.25-3.76	A	
1.6		1.43-3.84	A	
1.7		1.24-3.60	A	
1.8		1.15-3.28	A	
1.9		1.24-3.26	A	
2.0		1.34-3.30	A	

Table 3

Absolute coefficient values:
Ks = 0 Kb = 1305000 Cs = 240 Qs = 200000
eccentricity = .0000285 deadband = .000285 omega = varied

Nondimensionalizing parameters:
frequency = sqrt(Ks + Kb) = omega-naught = sqrt(1305000)
displacemtn = eccentricity = .0000285

Nondimensionalized coefficient values:
C = Cs/omega-naught = ND damping = 240/sqrt(1305000)
k = Ks/square(omega-naught) = ND stiffness = 1
B = Qs/square(omega-naught) = ND X-stiffness = 200000/1305000
phi = omega/omega-naught = ND forcing frequency = varied
delta = deadband/eccentricity = ND deadband = 10

phi	R	shape (A=annulus, C=circle)	
0.0	21.37	C	
0.1	21.36-21.39	A	annulus for phi
0.2	21.31-21.44	A	between 0.0 and 0.61
0.3	21.21-21.54	A	
0.4	21.03-21.72	A	
0.5	20.65-22.07	A	
0.6	19.63-22.94	A	
0.7	20.54	C	circle for phi
0.8	29.11	C	between 0.62 and 0.83
0.83 (PEAK)	32.40	C	
0.9	19.15-23.84	A	
1.0	19.69-23.15	A	annulus for phi
1.1	19.96-22.85	A	greater than 0.84
1.2	20.13-22.68	A	
1.3	20.23-22.58	A	
1.4	-	A	
1.5	-	A	
1.6	-	A	
1.7	20.45-22.69	A	
1.8	-	A	
1.9	-	A	
2.0	20.65-22.24	A	

Table 4

Absolute coefficient values:
  Ks = 0 Kb=1305000 Cs=240 Qs=200000
  eccentricity = .0000285 deadband = varied omega = varied.

Nondimensionalizing parameters:
  frequency = sqrt(Ks + Kb) = omega-naught = sqrt(1305000)
  displacement = eccentricity = .0000285

Nondimensionalized coefficient values:
  C = Cs/omega-naught = ND damping = 240/sqrt(1305000)
  k = Kb/square(omega-naught) = ND stiffness = 1
  B = Qs/square(omega-naught) = ND X-stiffness = 200000/1305000
  phi = omega/omega-naught = ND forcing frequency = varied
  delta = deadband/eccentricity = ND deadband = varied

deadband/eccentricity	circle/annulus regions
0.1	phi = 0.00 : circle
	0.01 <= phi <= 0.11 : annulus
	0.11 <= phi <= 4.00 : circle
0.5	phi = 0.00 : circle
	0.01 <= phi <= 0.23 : annulus
	0.24 <= phi <= 4.00 : circle
0.9	phi = 0.00 : circle
	0.01 <= phi <= 0.29 : annulus
	0.30 <= phi <= 4.00 : circle
1.0	phi = 0.00 : circle
	0.01 <= phi <= 0.31 : annulus
	0.32 <= phi <= 0.99 : circle
	1.00 <= phi <= 4.00 : annulus
2.0	phi = 0.00 : circle
	0.01 <= phi <= 0.40 : annulus
	0.41 <= phi <= 0.95 : circle
	0.96 <= phi <= 4.00 : annulus
5.0	phi = 0.00 : circle
	0.01 <= phi <= 0.53 : annulus
	0.54 <= phi <= 0.88 : circle
	0.89 <= phi <= 4.00 : annulus
10.0	phi = 0.00 : circle
	0.01 <= phi <= 0.61 : annulus
	0.62 <= phi <= 0.83 : circle
	0.84 <= phi <= 4.00 : annulus

Table 5

Same values as Table 4 except Kb = 700000 (this value is close to the instability boundary)

deadband/eccentricity	circle/annulus regions
0.1	Phi = 0.0 : circle
	0.01 <= Phi <= 0.15 : annulus
	0.16 <= Phi <= 4.00 : circle
0.5	Phi = 0.0 : circle
	0.01 <= Phi <= 0.32 : annulus
	0.33 <= Phi <= 4.00 : circle
0.9	Phi = 0.0 : circle
	0.01 <= Phi <= 0.42 : annulus
	0.43 <= Phi <= 4.00 : circle
1.0	Phi = 0.0 : circle
	0.01 <= Phi <= 0.44 : annulus
	0.45 <= Phi <= 0.99 : circle
	1.00 <= Phi <= 4.00 : annulus
2.0	Phi = 0.0 : circle
	0.01 <= Phi <= 0.59 : annulus
	0.60 <= Phi <= 0.99 : circle
	1.00 <= Phi <= 4.00 : annulus
5.0	Phi = 0.0 : circle
	0.01 <= Phi <= 0.86 : annulus
	0.87 <= Phi <= 0.99 : circle
	1.00 <= Phi <= 4.00 : annulus
10.0	Phi = 0.0 : circle
	0.01 <= Phi <= 0.98 : annulus
	Phi = 0.99 : circle

Table 6

Same values as Table 4 except Kb = 10 000 000 (an unusally large value for bearing stiffness, relative to the other parameters)

deadband/eccentricity	circle/annulus regions
0.1	phi = 0.0 : circle
	0.01 <= phi <= 0.04 : annulus
	0.05 <= phi <= 4.00 : circle
0.5	phi = 0.0 : circle
	0.01 <= phi <= 0.08 : annulus
	0.09 <= phi <= 4.00 : circle
0.9	phi = 0.0 : circle
	0.01 <= phi <= 0.10 : annulus
	0.11 <= phi <= 4.00 : circle
1.0	phi = 0.0 : circle
	0.01 <= phi <= 0.10 : annulus
	0.11 <= phi <= 0.99 : circle
	1.00 <= phi <= 4.00 : annulus
2.0	phi = 0.0 : circle
	0.01 <= phi <= 0.13 : annulus
	0.14 <= phi <= 0.94 : circle
	0.95 <= phi <= 4.00 : annulus
5.0	phi = 0.0 : circle
	0.01 <= phi <= 0.18 : annulus
	0.19 <= phi <= 0.83 : circle
	0.84 <= phi <= 4.00 : annulus
10.0	phi = 0.0 : circle
	0.01 <= phi <= 0.20 : annulus
	0.21 <= phi <= 0.52 : circle
	0.53 <= phi <= 4.00 : annulus

Table 7

Transitions between Bounded and Unbounded Regions

REAL [((Cs/2)**2 - (Ks+Kb) + iQs)**(1/2)] = Cs/2

Case: Cs = 150

Qs * 10**6	(Ks+Kb) * 10**6
.05	.112
.10	.444
.15	1.
.20	1.78
.25	2.78
.30	4.
.35	5.44
.40	7.11

Case: Cs = 240

Qs * 10 **6	(Ks+Kb) * 10**6
.05	.043
.10	.174
.15	.391
.20	.694
.25	1.085
.30	1.56
.35	2.13
.40	2.78